The Baroclinic Moisture Flux

RON MCTAGGART-COWAN

Numerical Weather Prediction Research Section, Environment and Climate Change Canada,
Dorval, Quebec, Canada

JOHN R. GYAKUM

Department of Atmospheric and Oceanic Sciences, McGill University, Montreal, Quebec, Canada

RICHARD W. MOORE

Norwegian Meteorological Institute, and Department of Meteorology and Oceanography,
University of Oslo, Oslo, Norway

ABSTRACT

As subsaturated air ascends sloping isentropic surfaces, adiabatic expansion results in cooling and relative moistening. This process is an effective way to precondition the atmosphere for efficient moist processes while bringing parcels to saturation, and thereafter acts to maintain saturation during condensation. The goal of this study is to develop a diagnostic quantity that highlights circulations and regions in which the process of parcel moistening by isentropic ascent is active. Among the many features that rely on this process for the generation of an important fraction of their energy are oceanic cyclones, transitioning tropical cyclones, warm conveyor belts, diabatic Rossby vortices, and predecessor rain events. The baroclinic moisture flux (BMF) is defined as moisture transport by the component of vertical motion associated with isentropic upgliding. In warm conveyor belt and diabatic Rossby vortex case studies, the BMF appears to be successful in identifying the portion of the circulation in which this process is actively bringing parcels to saturation to promote the formation of clouds and precipitation. On a broader scale, the climatological maxima of the BMF highlight regions in which parcel moistening by isentropic ascent is anticipated to have a nonnegligible impact on the atmospheric state either through the action of the mean flow or via the repeated occurrence of isolated large-BMF events. The process-centric foundation of the BMF makes it useful as a filtering or exploratory variable, with the potential for extension into predictive applications.

1. Introduction

Air parcel ascent along the sloping isentropic surfaces of a baroclinic zone leads to cooling and relative moistening by adiabatic expansion. (The term moistening is used hereafter to refer to increasing relative humidity within an air parcel during subsaturated ascent, and to the maintenance of saturation against specific humidity reductions once condensation occurs.) The process of parcel moistening by isentropic ascent preconditions the atmosphere to support the efficient production of clouds and precipitation, and is highly relevant to a range of atmospheric circulations that depend on latent heat release as an energy source. In this study, a diagnostic quantity called the baroclinic moisture flux (BMF) is developed to highlight this process and to identify features and regions in which it is active.

The phenomena of particular interest in this study are those in which strong baroclinicity and ample moisture supply coexist. It is for such flows that the process of parcel moistening by isentropic upgliding is likely to be of leading-order importance to the development and maintenance of the circulation. These features possess distinct spatial and temporal scales, but share important

process-level similarities. The BMF serves as a physically based connection between such circulations, examples of which are introduced in more detail here.

Oceanic cyclones, in particular those that intensify rapidly over relatively warm currents and coastal waters (Sanders and Gyakum 1980; Roebber 1984; Yoshida and Asuma 2004), rely heavily on latent heat released during the formation of clouds and precipitation to create the lower-level potential vorticity maximum that characterizes the circulation (Bosart 1981; Kuo et al. 1991; Davis and Bosart 2003; Hirata et al. 2015). Although these storms frequently also benefit from cyclonic vorticity advection aloft (Plant et al. 2003), Shapiro and Keyser (1990) present an example of a development that follows closely the type-A classification of Petterssen and Smebye (1971). The bulk of cloud formation in these systems occurs in the ascending portion of the warm conveyor belt as air parcels rise along the steeply sloped isentropes of the warm front (Carlson 1980; Browning 1990; Wernli 1997; Eckhardt et al. 2004; Madonna et al. 2014), the vertical angle of which is itself a measure of the potential for moist baroclinic growth (Papritz and Spengler 2015). The water vapor available for condensation in such airstreams depends strongly on the humidity of the source region (Pfahl et al. 2014), leading to the definition of tropical moisture exports by Knippertz and Wernli (2010) and Knippertz et al. (2013) as flows that transport parcels from the tropics into the midlatitudes. Knippertz and Wernli (2010) link these transports to identifiable features known to produce heavy precipitation. These Lagrangian perspectives of the slantwise ascent of airstreams of tropical and subtropical origin partially overlap with the Eulerian definition of atmospheric rivers by Zhu and Newell (1998) as narrow plumes of enhanced precipitable water associated with large values of instantaneous poleward water vapor transport (Lackmann et al. 1999; Ralph et al. 2004, 2011; Lavers et al. 2011). Sodemann and Stohl (2013) connect these viewpoints to suggest that multiple cyclones can interact with an atmospheric river, both contributing to its longevity and tapping the moisture available within it.

Parcel moistening by isentropic ascent is also an essential process for diabatic Rossby vortices [Parker and Thorpe (1995), Moore et al. (2013), and references therein, also denoted "diabatic Rossby waves" as discussed by Boettcher and Wernli (2013)]. Isentropic upgliding downshear of the circulation center leads to the continual generation of cyclonic potential vorticity ahead of the system, thus to the characteristic rapid progression of the storm during the propagation phase of its life cycle. By contrast, the persistent ascent of warm, moist air advected poleward in the outer circulation of a tropical cyclone across a preexisting baroclinic zone can lead to the formation of a stationary region of heavy precipitation known as a predecessor rain event (Galarneau et al. 2010). This feature is distinct from the tropical cyclone remnant, which may itself be associated with widespread precipitation as it develops the baroclinic airstreams associated with an extratropical cyclone from an initially tropical air mass (Jones et al. 2003; Evans and Hart 2008). Tropical cyclone–like features are sometimes also observed at higher latitudes, where cloud structures in polar lows and Mediterranean cyclones are evidence of ascent across strong frontal zones while convection near the storm center is indicative of the leading impact of diabatic processes on the formation and maintenance of the circulation (Rasmussen 1979; Emanuel 2005).

Although baroclinicity tends to be weaker in the tropics than in the midlatitudes, isentropic upgliding in the subtropical precipitation zones leads to the development of quasi-stationary regions of clouds at lower latitudes (Kodama 1992). These features owe their existence in part to the influence of monsoon systems, seasonal circulations associated with moisture transports, and surface fluxes in baroclinic low-level jets (Higgins et al. 1997; Vera et al. 2006; Boos and Emanuel 2009). The influences of diurnal heating and orography can lead to strong moist ageostrophic flows near the equator (Cook 1999), the isallobaric component of which is directly related to isentropic vertical displacements and attendant moistening (Carroll 2003).

The goal of this study is to design a diagnostic quantity that is capable of highlighting the process of parcel moistening by isentropic ascent that connects the apparently disparate features described above. The focus on the component of vertical motion related to isentropic upgliding provides the process-centric foundation for the BMF as developed in section 2, and distinguishes it from measures of moisture field morphology such as moisture convergence and integrated vapor transport (Benton and Estoque 1954; Rasmusson 1967). The application of the BMF to archetypal warm conveyor belt and diabatic Rossby vortex cases in section 3 outlines the properties of the diagnostic in a simplified context. In section 4, a climatology of the BMF shows the quantity to be successful both in highlighting regions in which moistening by isentropic ascent is known to be active, and in identifying areas in which this process may be associated with understudied circulations. The potential for the BMF to serve simultaneously as a filtering,[1] exploratory, and predictive quantity is discussed in section 5.

---

[1] The term "filtering" is used here to describe the ability of the BMF to distinguish between systems whose dry structures are similar, based on the relative importance of moist processes to the development and maintenance of the circulation.

2. Development of the BMF

The foundation for the BMF is the simple expression of the vertical transport of moisture, with the process-oriented focus of the diagnostic arising from the replacement of the full vertical motion with the component related to isentropic upgliding. Computation of the latter requires knowledge of the synoptic steering velocity, a quantity that is difficult to estimate in general. Each of these elements must be considered during the development of the BMF as outlined in sections 2a–d. Throughout this study, isobaric data from the European Centre for Medium-Range Weather Forecasts (ECMWF) interim reanalysis (ERA-Interim) project on a 1.5° grid is employed for calculations (Dee et al. 2011) over the 1989–2014 period. This well-studied dataset has sufficient resolution to depict accurately the features of interest to this investigation despite uncertainty in the water vapor field, particularly over the oceans (Trenberth et al. 2011).

a. The BMF as a vertical moisture transport

We begin with the definition of the three-dimensional water vapor transport, which can also be interpreted as the water vapor flux ($\mathbf{F}$) through a unit area oriented normal to the flow:

$$\mathbf{F} = \mathbf{F}_h + \mathbf{F}_z = \mathbf{V}q + \hat{k}wq, \qquad (1)$$

where subscripts h and z refer to the horizontal and vertical directions, respectively; $\mathbf{V}$ and w refer to the horizontal and vertical winds, respectively; and q is the specific humidity (all symbols are defined in Table 1 for reference). The integrated vapor transport can then be defined as the mass-weighted vertical integral of $\mathbf{F}_h$, a well-studied quantity that effectively describes the evolution of the large-scale structure of the moisture field. Although the vertical component of the moisture flux is generally one to two orders of magnitude smaller than its horizontal counterpart, $\mathbf{F}_z$ may be closely related to sensible weather because of the relative moistening of parcels implied by the positive $\mathbf{F}_z$ values found in ascending moist airstreams. Treating the vertical component in isolation, thus dropping vector notation,

$$F_z = wq \approx \left(\frac{-RT}{gp}\right)\omega q, \qquad (2)$$

with the hydrostatic approximation applied to switch from height- to pressure-based vertical motion (w to ω).

Although the vertical motion field can be obtained directly from analyses or a primitive equation model, this ω contains contributions from numerous sources

TABLE 1. List of symbols used in this study.

Symbol	Description
∇_h	Horizontal gradient operator
Γ	Vertical motion component ratio
$\hat{\Gamma}$	Vertical motion component ratio in a stationary reference frame ($\mathbf{C} = 0$)
θ	Dry air potential temperature
ρ_w	Density of water
σ	Dry static stability
σ_m	Moist static stability
ω	Vertical motion in isobaric coordinates
ω_{ID}	Component of ω related to isentropic displacement
$\hat{\omega}_{\mathrm{ID}}$	Isentropic displacement ω component in a stationary reference frame ($\mathbf{C} = 0$)
ω_{IU}	Component of ω related to isentropic upgliding
$\hat{\omega}_{\mathrm{IU}}$	Isentropic upglide ω component in a stationary reference frame ($\mathbf{C} = 0$)
$\mathcal{B}$	Baroclinic moisture flux (BMF)
$\tilde{\mathcal{B}}$	Vertically integrated BMF (from p_b to p_t)
$\mathbf{C}$	Steering velocity (reference frame displacement)
c_p	Specific heat at constant pressure
$\mathbf{F}$	Moisture flux
$\mathbf{F}_h$	Horizontal component of moisture flux
$\mathbf{F}_z$	Vertical component of moisture flux
g	Gravitational acceleration
p	Air pressure
p_b	Air pressure of lower bound of $\mathcal{B}$ (850 hPa)
p_t	Air pressure of upper bound of $\mathcal{B}$ (250 hPa)
q	Specific humidity
q_s	Saturation specific humidity
$\mathcal{R}$	Relative humidity
R	Gas constant for dry air
s_χ	Temperature gradient operator for steering velocity estimate [Eqs. (13) and (14)]
T	Dry air temperature
$\mathbf{V}$	Horizontal wind vector
$\mathcal{V}$	System volume for best estimate of steering velocity
w	Vertical motion in height coordinates

(forcings). Because it is the goal of this study to identify areas in which isentropic upgliding is acting to bring parcels toward saturation, it is necessary to filter out vertical motions associated with processes not directly related to this physical process. An estimate of the component of the vertical motion field associated with isentropic upgliding (ω_{IU}) will, therefore, replace the full ω in Eq. (2) to serve as the basis for the development of the BMF ($\mathcal{B}$), which is now defined as follows:

$$\mathcal{B} \equiv \left(\frac{-RT}{gp}\right)\omega_{\mathrm{IU}}q. \qquad (3)$$

The applicability of this definition depends on the availability of a reliable estimate of ω_{IU}, the calculation of which is the subject of section 2c following an investigation of the relationship of the BMF to the relative moistening of air parcels.

b. Relative moistening by the BMF

Despite its formulation as a component of the vertical moisture flux, it is the relationship between the BMF and the process of parcel moistening by isentropic ascent that is essential to the utility of Eq. (3). The evolution of the relative humidity ($\mathcal{R} = q/q_s$, where q_s is the saturation specific humidity) in a parcel is described using the Lagrangian derivative as follows:

$$\frac{d\mathcal{R}}{dt} = \frac{d}{dt}\left(\frac{q}{q_s}\right) = \frac{1}{q_s}\frac{dq}{dt} - \frac{\mathcal{R}}{q_s}\frac{dq_s}{dT}\frac{dT}{dt}. \quad (4)$$

The first term on the right-hand side of Eq. (4) represents the effect of evaporation or condensation on $\mathcal{R}$, while the second term describes the influence of adiabatic temperature changes. To cast the latter in a form that is directly applicable to this investigation, the first law of thermodynamics and ideal gas laws are combined to describe adiabatic temperature changes in parcels undergoing vertical displacements:

$$c_p\frac{dT}{dt} - \frac{1}{\rho}\frac{dp}{dt} = 0 \quad \text{and} \quad \frac{dT}{dt} = \frac{RT}{c_p p}\omega,$$

which can be combined with Eq. (4) to yield the following:

$$\frac{d\mathcal{R}}{dt} = \frac{1}{q_s}\frac{dq}{dt} - \frac{RT}{c_p p q_s^2}\frac{dq_s}{dT}\omega q, \quad (5)$$

in which a form of the vertical moisture flux [Eq. (2)] is clearly identifiable in the adiabatic term. Replacing the full vertical motion field in Eq. (5) with the component related to displacements along isentropic surfaces as in the previous section allows for the direct substitution of the BMF [Eq. (3)] such that

$$\frac{d\mathcal{R}}{dt} = \frac{1}{q_s}\frac{dq}{dt} + \frac{g}{c_p q_s^2}\frac{dq_s}{dt}\mathcal{B}. \quad (6)$$

This formulation relates changes in $\mathcal{R}$ directly to the BMF because of the positive-definite nature of the temperature-dependent factor that precedes the BMF in the adiabatic term. Equation (6) remains valid under conditions of both dry and moist ascent to the extent that the BMF can be adequately diagnosed when moist processes are active, a caveat that is discussed in section 5. Prior to saturation in an ascending airstream, $dq/dt = 0$ as specific humidity is conserved in the air parcel, such that $\mathcal{B} > 0$ leads directly to relative moistening ($d\mathcal{R}/dt > 0$) by cooling resulting from adiabatic expansion. Once the air parcel becomes saturated, $\mathcal{R} = 1$ and $d\mathcal{R}/dt = 0$ so that the two terms on the right-hand side of Eq. (6) must be in balance[2] and $\mathcal{B} > 0$ is required to compensate for condensation-induced specific humidity reduction ($dq/dt < 0$). Physically, $\mathcal{B} > 0$ is, therefore, indicative of relative moistening both before and after the onset of condensation in an ascending airstream: it increases $\mathcal{R}$ in the former case and maintains saturation against the effects of condensation in the latter.

c. Diagnosing isentropic upglide

The value of ω_{IU} is not typically known for analysis or model datasets. However, both Hoskins et al. (2003) and Carroll (2003) develop a method for diagnosing this component of vertical motion. Following generally the derivation of Hoskins et al. (2003), we begin with the adiabatic form of the thermodynamic equation in isobaric coordinates:

$$\frac{\partial T}{\partial t} = -\mathbf{V} \cdot \nabla_h T + \omega\sigma\frac{p}{R},$$

where $\sigma = -(RT/p)(\partial \ln\theta/\partial p)$ represents dry static stability, which we assume to be greater than zero throughout the remainder of the analysis. Rearranging to solve for vertical motion results in the following:

$$\omega = \left(\frac{\partial T}{\partial t} + \mathbf{V} \cdot \nabla_h T\right)\bigg/\left(\frac{\sigma p}{R}\right). \quad (7)$$

Employing the assumption that the isentropic structures of the synoptic-scale environment are at steady state, Green et al. (1966) define a system motion ($\mathbf{C}$) that represents the horizontal translation velocity of a fixed isentropic pattern. As demonstrated by Namias (1939), the relatively long time scales of synoptic development compared to those of parcel displacements within a system make this assumption a fundamental tenet of isentropic analysis that remains qualitatively valid even during rapidly evolving events (Browning 1990). System motion is represented by the introduction of a translation component in Eq. (7) as follows:

$$\omega = \left[\frac{\partial T}{\partial t}\bigg|_{\mathbf{C}} + (\mathbf{V} - \mathbf{C}) \cdot \nabla_h T\right]\bigg/\left(\frac{\sigma p}{R}\right). \quad (8)$$

The horizontal Galilean invariance of ω implies that Eqs. (7) and (8) are mathematically identical.

---

[2] Although in-cloud heterogeneity is clearly observed (Larson et al. 2001) and some degree of transient supersaturation may be present particularly near cloud base (Korolev and Maxin 2003), the equilibrium assumption remains sufficient for this conceptual discussion.
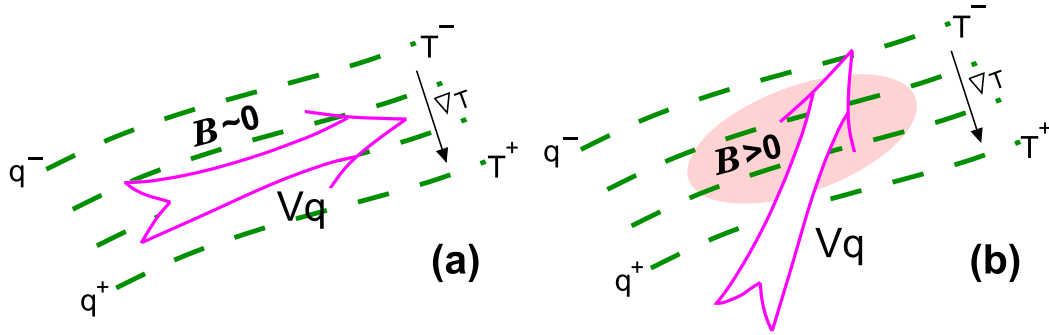
FIG. 1. A conceptual diagram of BMF structures associated with moisture transport in a simple baroclinic environment without translation ($\mathbf{C} = 0$). Horizontal vapor transport ($\mathbf{V}q$) is shown with a large magenta arrow, with background isotherms and isohumes denoted using dashed dark green lines (gradient vectors directed toward the lower-right corner of the page). (a) Transport along the baroclinic zone yields $\mathcal{B} \approx 0$. (b) The component of flow parallel to the environmental gradients yields a region of $\mathcal{B} > 0$ indicated with pink shading.

The first term on the right-hand side of Eq. (8) represents the time evolution of the isentropic pattern in the system-following reference frame, and thus represents the deviation from the assumption of a fixed translating structure. Its consideration in isolation leads to the definition of the "isentropic displacement" component of vertical motion:

$$\omega_{\mathrm{ID}} = \left(\frac{R}{\sigma p}\right) \frac{\partial T}{\partial t}\bigg|_{\mathbf{C}}, \tag{9}$$

which is small only if the system evolves slowly in the chosen reference frame.

The second term of the right-hand side of Eq. (7) is of more direct relevance to the derivation of the BMF because it represents the component of vertical motion associated with the movement of parcels along sloping isentropic surfaces as follows:

$$\omega_{\mathrm{IU}} = \left(\frac{R}{\sigma p}\right)(\mathbf{V} - \mathbf{C}) \cdot \nabla_h T. \tag{10}$$

The full vertical motion is the sum of the isentropic displacement [Eq. (9)] and upglide [Eq. (10)] components, thus $\omega = \omega_{\mathrm{ID}} + \omega_{\mathrm{IU}}$.

This definition of ω_{IU} provides the missing ingredient required to complete the derivation of the BMF. Substitution of Eq. (10) into Eq. (3) yields the following:

$$\mathcal{B} = \frac{-1}{\sigma} \left(\frac{R^2 T}{g p^2}\right) \nabla_h T \cdot (\mathbf{V} - \mathbf{C})q. \tag{11}$$

This form of the BMF illustrates the focus of the diagnostic on the isentropic ascent of humid air parcels as shown in Fig. 1. The transport of parcels parallel to a baroclinic zone is associated with a null BMF field (Fig. 1a). For a flow angled into the baroclinic zone,

however, the component of the wind directed against the thermal gradient contributes to positive BMF as moisture is transported vertically along the sloping isentropes (Fig. 1b). Ideal conditions for large positive BMF values, therefore, consist of strong warm advection in the presence of ample moisture, a description that aligns well with the conceptual models of features for which moist isentropic ascent is a dominant process.

The treatment of moisture in Eq. (11) leads to an asymmetry in the interpretation of BMF extremes. Peak negative BMF values are associated with the isentropic downgliding of moist parcels: dry environments possess small absolute BMF values by construction. Large negative BMF values are, therefore, indicative of regions in which the relative drying of parcels by adiabatic vertical motions leads to the suppression of clouds and precipitation in an otherwise-favorable air mass.

Further asymmetry in the BMF field may arise from the typical relative orientations of thermal gradients and reference frame displacement ($\mathbf{C}$) as shown in Fig. 2. Similar absolute magnitudes of temperature advection occur along the warm and cold fronts of an idealized midlatitude cyclone in the stationary reference frame (Fig. 2a). However, the advection pattern associated with reference frame displacement (Fig. 2b) displays marked asymmetry due to the alignment of $\mathbf{C}$ with the baroclinic zone in the warm frontal region only. The system-relative advection structure (Fig. 2c) reflects this asymmetry, with strong storm-relative warm advection along the warm front and weak storm-relative cold advection along the cold front. These advection patterns have a direct influence on the BMF [Eq. (11)] because of its sensitivity to isentropic upgliding in the translating reference frame. They also demonstrate that the definition of $\mathbf{C}$, discussed in more detail in the next section, will have a larger impact in regions where baroclinic
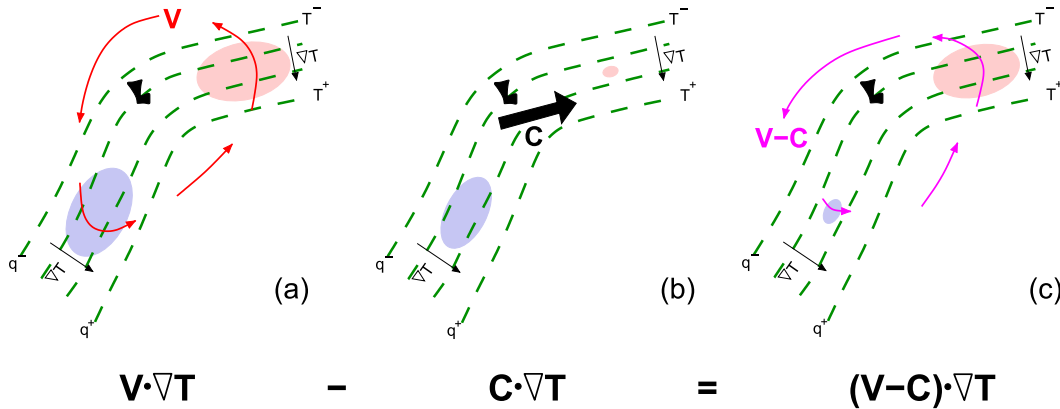
FIG. 2. A conceptual diagram of thermal advection structures associated with a typical eastward-moving frontal cyclone for the (a) full wind, (b) system velocity, and (c) storm-relative flow, where the difference (a) − (b) yields (c) as shown across the bottom of the plot. Background isotherms and isohumes are plotted using dashed dark green lines as in Fig. 1. The full cyclonic flow (**V**) around the low pressure center (black bold somewhat L-looking symbol) is shown using curved red arrows, while the system displacement vector is denoted **C** in association with the large black arrow. Pink shading is indicative of regions of warm advection, while light blue shading represents areas of cold advection by the relevant vector quantity in each panel. Patch sizes are indicative of the relative magnitude of advection.

zones are perpendicular to system motion than it will in areas where the two are aligned.

The integral form of the BMF ($\tilde{\mathcal{B}}$) is defined by vertical integration:

$$\tilde{\mathcal{B}} = \frac{1}{g\rho_w} \int_{p_b}^{p_t} \mathcal{B} \, dp, \qquad (12)$$

where the limits of integration used here ($p_b = 850$ hPa and $p_t = 250$ hPa; though results are qualitatively insensitive to reasonably changes in these values) represent the approximate depth of the free troposphere. It is this form of the BMF that will be employed for the remainder of this investigation.

d. Estimating the synoptic steering velocity

The definition of the BMF in Eq. (11) relies on an estimate of the translation of the reference frame (**C**), a "synoptic steering velocity" that represents system motion. Hoskins et al. (2003) propose an objective method for determining **C** based on ω_{IU} and ω_{ID} in the quasigeostrophic framework with **V** replaced by the geostrophic wind in Eq. (7). The BMF itself does not intrinsically rely on this simplification, and can be freed from it completely if an alternative steering velocity estimate is employed as discussed at the end of this section.

Key to the Hoskins et al. (2003) determination of **C** are the facts that the full quasigeostrophic ω field is Galilean invariant and that the optimal displacement velocity for a system-following reference frame is the one in which the isentropes undergo minimal deformation over time. The latter implies that the time tendency of temperature in the translating reference

frame is a minimum, as is ω_{ID} through Eq. (9). This can be expressed as the minimization of ω_{ID}^2 over a volume ($\mathcal{V}$) of the atmosphere representative of synoptic-scale features of interest. Hoskins et al. (2003) show that the unique solution to this variational problem is obtained analytically when the components of the synoptic steering velocity $\mathbf{C} = (c_x, c_y)$ are solutions of the linear system:

$$\begin{pmatrix} \int s_x^2 \, d\mathcal{V} & \int s_{x,y} \, d\mathcal{V} \\ \int s_{x,y} \, d\mathcal{V} & \int s_y^2 \, d\mathcal{V} \end{pmatrix} \begin{pmatrix} c_x \\ c_y \end{pmatrix} = -\begin{pmatrix} \int s_x \hat{\omega}_{\text{ID}} \, d\mathcal{V} \\ \int s_y \hat{\omega}_{\text{ID}} \, d\mathcal{V} \end{pmatrix}, \qquad (13)$$

where $s_\chi = (R/\sigma p)(\partial T/\partial \chi)$ and $\hat{\omega}_{\text{ID}}$ is ω_{ID} from Eq. (9) with $\mathbf{C} = 0$, a value that can be computed diagnostically as $\omega - \hat{\omega}_{\text{IU}}$ from standard gridded data using Eq. (10) with $\mathbf{C} = 0$. Substitution to eliminate c_y yields a direct solution:

$$c_x = \frac{\int s_y \hat{\omega}_{\text{ID}} \, d\mathcal{V} - \left(\dfrac{\int s_y^2 \, d\mathcal{V}}{\int s_{x,y} \, d\mathcal{V}} \right) \int s_x \hat{\omega}_{\text{ID}} \, d\mathcal{V}}{\int s_{x,y} \, d\mathcal{V} - \dfrac{\int s_x^2 \, d\mathcal{V} \int s_y^2 \, d\mathcal{V}}{\int s_{x,y} \, d\mathcal{V}}}, \qquad (14)$$

the result of which can be used to compute c_y by back-substitution into Eq. (13).

This framework effectively identifies the translation speed of the reference frame that minimizes the deformation of

isentropes in the volume of interest, but does not provide a quantitative assessment of the relative importance of the components of quasigeostrophic vertical motion. Hoskins et al. (2003) propose a nondimensional index based on the ratio of the squares of the estimated components:

$$\Gamma = \frac{\int \omega_{\mathrm{ID}}^2 \, d\mathcal{V}}{\int \omega_{\mathrm{IU}}^2 \, d\mathcal{V}}, \qquad (15)$$

which provides a measure of the importance of ω_{ID} relative to ω_{IU} within the volume of interest. A value of Γ smaller than unity is indicative of a volume in which isentropic upgliding is largely responsible for quasigeostrophic vertical motion, while larger values occur in regions in which the configuration of the flow is changing rapidly even from the perspective of the optimally translating reference frame. The impact of ignoring system motion can be assessed by comparing Γ with its counterpart computed with $\mathbf{C} = 0$:

$$\hat{\Gamma} = \frac{\int \hat{\omega}_{\mathrm{ID}}^2 \, d\mathcal{V}}{\int \hat{\omega}_{\mathrm{IU}}^2 \, d\mathcal{V}}, \qquad (16)$$

where $\Gamma \leq \hat{\Gamma}$ by construction. This assertion is true for the climatological values of $\hat{\Gamma}$ and Γ shown in Fig. 3. Moreover, Γ remains well below unity in all regions outside of the tropics, a result that illustrates the effectiveness of Eq. (13) at latitudes where quasigeostrophic balance is expected to be valid. The associated steering velocities (Fig. 3b) peak below the mean polar jets with regionally enhanced values over the Northern Hemisphere oceans. The tropical easterlies lead to easterly steering within 15° of the equator (Sadler 1975), consistent with the displacement of features in this region (Hennon et al. 2013) and indicative of the relevance of the Hoskins et al. (2003) framework even at low latitudes.

Despite the elegance of the computation of the synoptic steering velocity proposed by Hoskins et al. (2003), it relies on both the validity of quasigeostrophic assumptions and the definition of an appropriate synoptic-scale volume of interest ($\mathcal{V}$), both of which indirectly influence the final value of the BMF through $\mathbf{C}$ [Eq. (11)]. In this study, volume integrals are computed using a 5° radius through the depth of the free troposphere (850–250 hPa) for consistency with Eq. (12). Although the results of this study are qualitatively insensitive to reasonable changes in $\mathcal{V}$, simpler estimates of $\mathbf{C}$ that do not rely on volume integrals do not require this definition. The applicability of $\mathbf{C} = 0$ will, therefore, also be considered in this study, representative of a
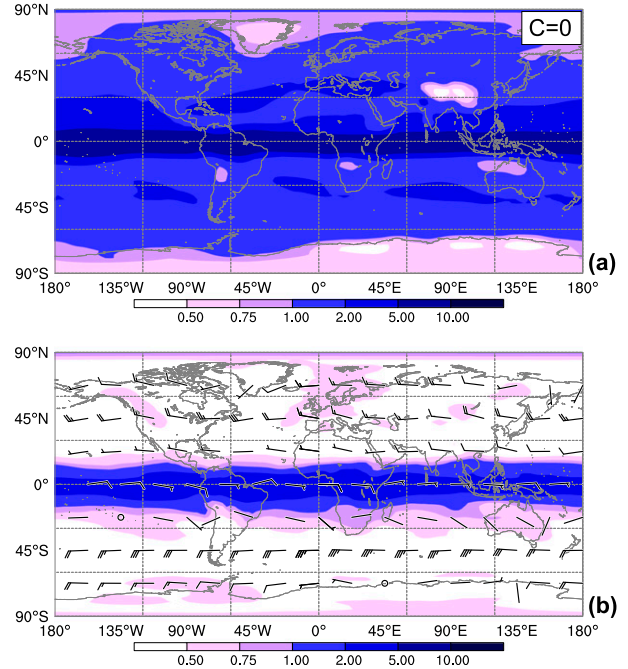

FIG. 3. Mean climatological values (1989–2015) of tropospheric (a) $\hat{\Gamma}$ and (b) Γ [Eqs. (16) and (15), respectively] are color shaded as indicated on the color bar. For consistency with the volume integrals employed later in the study, a 5° radius is used throughout the 850–250-hPa layer to represent the free-tropospheric environment. The associated synoptic steering velocity is plotted with wind barbs in (b), where short, long, and pennant barbs represent steering speeds (|$\mathbf{C}$|) of 5, 10, and 50 kt, respectively.

geographically fixed reference frame as employed by Papritz and Spengler (2015) for their study of isentropic slopes. This simplification will facilitate the comparison of BMF conceptual models and case study results in section 3. Moreover, the adoption of $\mathbf{C} = 0$ may be justified for the evaluation of BMF for topographically anchored features that do not move with the synoptic steering flow. In such cases, the use of a geographically fixed reference frame may be more physically appropriate. Further possibilities for alternative definitions of $\mathbf{C}$ that do not rely on volume integrals, including those based on nondivergent winds at the equivalent barotropic level (Held et al. 1985) and midtropospheric winds (Simmonds et al. 1999; Pfahl et al. 2015), and their impacts on estimates of isentropic upgliding and the BMF will be the subject of a future investigation.

3. The BMF for canonical cases

The BMF associated with a pair of well-documented synoptic-scale features that rely heavily on isentropic upgliding for the formation of clouds and precipitation is described in this section: a warm conveyor belt and a diabatic Rossby vortex. The diagnoses of these canonical

features forms the basis for analyses of the BMF field of more complex structures for which the underlying process-based principles remain the same.

a. Warm conveyor belt

The warm conveyor belt circulation of an extra-tropical cyclone can transport moisture horizontally from the tropics to the midlatitudes, where isentropic upgliding in the head region leads to the formation of clouds and precipitation. This conceptual model is shown diagrammatically in Fig. 4, based on a simplified representation of the airstreams associated with a typi-cal extratropical cyclone (Carlson 1980; Browning 1985). Despite large integrated vapor transport in the warm conveyor belt as warm, humid air parcels move poleward ahead of the trailing cold front, the BMF in this region remains small because the flow is generally parallel to the baroclinic zone (ana- and kata-type cold fronts may be associated with local positive and negative BMF values, respectively). When these parcels reach the head of the warm conveyor belt, they ascend the sloping isentropes in the warm frontal zone and the BMF be-comes strongly positive as a reflection of their relative moistening by adiabatic expansion. It is in this region that the bulk of cloud formation and precipitation occurs.

In typical oceanic systems, the cold conveyor belt possesses moisture acquired by parcels as they move beneath the warm frontal surface (Grotjahn and Wang 1989; Kain et al. 2000). The majority of parcels in this airstream curl cyclonically around the low pressure center to arrive behind the cold front (Schultz 2001), where they undergo isentropic downgliding in the 1–4-km layer (Browning and Roberts 1994), the upper portion of which contributes to the weak negative maximum of the BMF shown in Fig. 4. Parcels in the dry airstream (Carlson 1980) have their origins aloft and possess little moisture as they descend behind the cold front and as-cend in the warm frontal zone. The dry airstream thus contributes very little negative BMF to the system, al-though any mixing with warm conveyor belt air would reduce the amplitude of the maximum positive BMF in the ascent region.

The validity of this simple description of the warm conveyor belt BMF structure is evaluated using a case of extreme Norwegian precipitation (Stohl et al. 2008). The September 2005 event began with a meridionally ex-tended axis of enhanced moisture, established in the eastern North Atlantic basin by Hurricanes Nate and Maria. The posttropical Maria merged with a preexisting circulation over the Norwegian Sea and was locally re-named Kristin before bringing record rainfalls to western Norway early on 14 September 2005. Stohl et al. (2008) show large precipitation rates over the northeastern
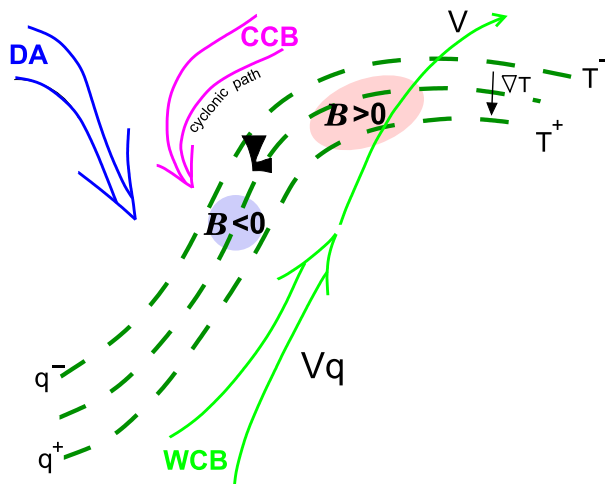

FIG. 4. Diagram of the conceptual model of moisture transport by a warm conveyor belt, including estimates of the associated BMF ($\mathcal{B} > 0$ in pink shading and $\mathcal{B} < 0$ in light blue shading, with patch sizes representative of magnitude). Isotherms associated with the cyclone center (black bold somewhat L-looking symbol) are plotted with dashed dark green lines, and are assumed to co-incide with isohumes such that both gradient vectors point to the bottom-right of the plot. The main cyclone airstreams are shown with large open arrows and labeled as dry airstream (DA; blue), cyclonic path of the cold conveyor belt (CCB; magenta), and warm conveyor belt (WCB; green). The largest magnitude of the mois-ture transport vector ($\mathbf{V}q$) is coincident with the WCB, while the ascending portion of the WCB is shown with an arrow labeled V crossing the baroclinic zone.

North Atlantic Ocean on 12–13 September, associated with the release of moisture acquired primarily by tur-bulent surface fluxes in the tropics and subtropics over the preceding week (their Figs. 9 and 10). This pre-cipitation in the head region of the warm conveyor belt was locally enhanced by orographic lifting, lead-ing to the highly efficient extraction of water vapor from parcels brought toward saturation by isentropic ascent.

The positive BMF structure over Scotland and the Norwegian Sea at 1800 UTC 13 September 2005 (Fig. 5a) bears a strong resemblance both to the con-ceptual model (Fig. 4) and to the oceanic component of the trajectory-based water vapor budget analysis of Stohl et al. (2008) (their Fig. 9a). With the exception of a pair of disturbances in the central Atlantic, the axis of moisture transport that extends from the subtropics to-ward Norway possesses small BMF values, consistent with flow parallel to the baroclinic zone. Parcels with their origins in the subtropics rise from the lower tro-posphere as they move poleward in this southwesterly flow beneath the dry airstream (Fig. 6). Those with their origins closest to Maria's remnant at 1800 UTC 10 Sep-tember (the beginning of the 72-h back trajectories
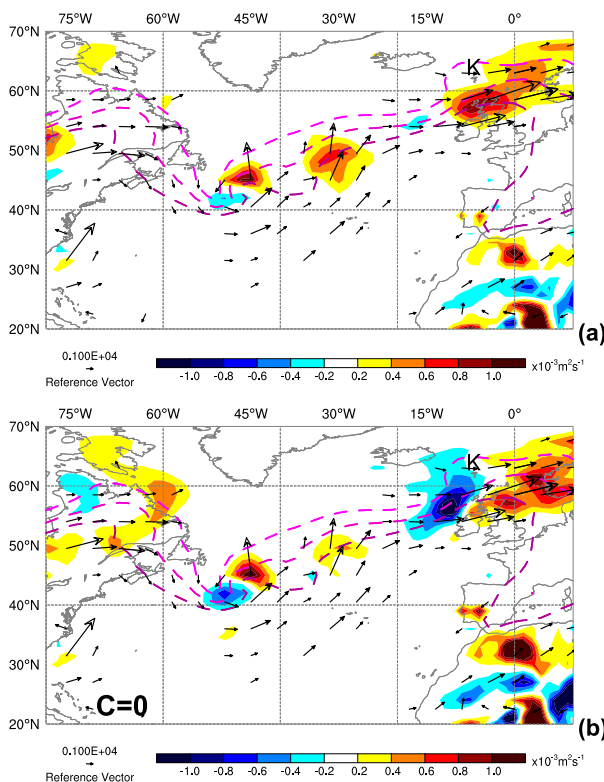
FIG. 5. Free-tropospheric BMF for 1800 UTC 13 Sep 2005 (850–250 hPa; color shaded as indicated on the color bar), integrated vapor transport (850–250 hPa; vector lengths scaled according to the reference vector), and 1000–500-hPa thickness (dashed contours for 5520, 5580, and 5640 m with lighter magenta colors for smaller thicknesses). The BMF computed with (a) the best estimate of **C** and (b) **C** = 0. The position of cyclone Kristin is indicated with a K near the top right of each panel.
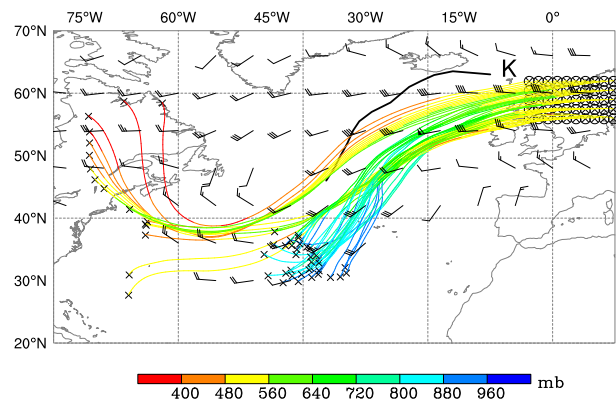

FIG. 6. Back-trajectories for parcels at 500 mb in the peak BMF region at 1800 UTC 13 Sep 2005 (Fig. 5). Trajectories are plotted for a 72-h period (1800 UTC 10 Sep–1800 UTC 13 Sep), with start points identified with an × symbol and end points with an × symbol within a circle, and are color shaded by pressure level as indicated on the color bar. The final time (1800 UTC 13 Sep) synoptic steering flow is plotted with wind barbs using the same convention as in Fig. 3, with barbs plotted only in regions where the steering flow exceeds 10 kt for readability. The position of cyclone Kristin at 1800 UTC 13 Sep is indicated with a K near the top right while the positions of Maria's extratropical remnant from the National Hurricane Center's best track over the 72-h period leading up to this time is shown with a solid black line.

shown in Fig. 6) undergo rapid moist ascent along the ana front on 11 September, increasing their potential temperatures by approximately 10 K in 24 h (red parcels in Fig. 7). A positive BMF over this period allows the relative humidity in the airstream to remain generally greater than 60%, sufficient to sustain partial cloudiness at midlevels (Quaas 2012) despite the depletion of specific humidity by condensation, an illustration of the impact of the BMF during moist ascent described in section 2b. Parcels that originate farther south of Maria's remnant (green parcels in Fig. 7) ascend primarily adiabatically on 11 September, with relative humidity increasing through isentropic upgliding (positive BMF values) while potential temperature and specific humidity remain relatively constant. The BMF values in this airstream increase dramatically on 13 September as parcels approach the head region of the warm conveyor belt and undergo rapid moist ascent.

The importance of orographic precipitation enhancement suggests that the adoption of **C** = 0 may be

physically justified in this case (Fig. 5b). The adoption of the stationary reference frame yields a BMF field with maxima that are more focused on the topographical features along the Norwegian coast. The strengthened negative BMF pattern west of the British Isles results from the use of **C** = 0 in a region where thermal gradients project strongly onto system displacement (section 2c and Fig. 2); physically, this leads to strong isentropic downgliding in the fixed reference frame. However, from the perspective of identification of heavy-rain regions resulting from ascent in the warm conveyor belt, the fixed reference frame appears to be effective for this event.

b. Diabatic Rossby vortex

Diabatic Rossby vortices are small, fast-moving cyclonic circulations for which parcel moistening by isentropic ascent is an essential process. Parker and Thorpe (1995) propose a conceptual model for the propagation phase of the system life cycle that involves the continuous generation of cyclonic potential vorticity beneath active convection as the induced circulation impinges on a lower-level baroclinic zone (their Fig. 6). Both the genesis and propagation phases of the life cycle are shown in Fig. 8 from the perspective of the BMF.

The development of the system depends on the presence of a cross-isentropic flow of relatively warm, moist air as depicted in Fig. 8a. This structure can arise as a result of subtropical circulations impinging on a midlatitude
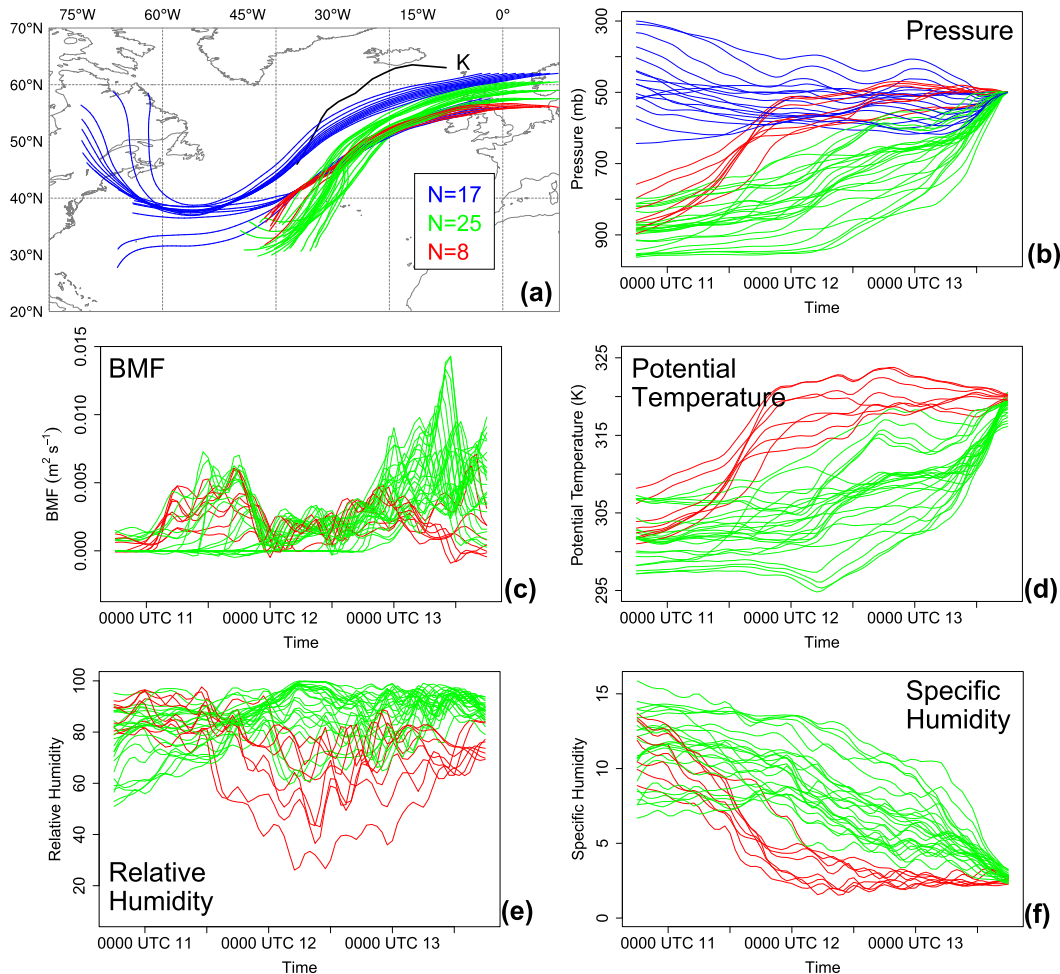
FIG. 7. Parcel properties along the trajectories shown in Fig. 6, separated into airstreams based on ascent properties: dry airstream (blue), rapid ascent (red), and warm conveyor belt (green) (further details provided at the end of the caption). (a) The spatial distribution and count (*N*) of airstream parcels is shown along with storm tracks as shown in Fig. 6. (b)–(f) The evolution of parcel properties over the 72-h period of the trajectory analysis, as indicated in the individual panels. Only parcels in the ascending airstreams are plotted in moisture-relevant panels in (c)–(f) for readability. The BMF in the boundary layer (below p_b) is set to zero to avoid plotting unrepresentative values obtained with the free-tropospheric steering flow for parcels near the surface. Dry airstream parcels begin their paths above the 700-mb level at 1800 UTC 10 Sep (blue), while those classified as "rapid ascent" rise above 600 mb by 0000 UTC 12 Sep (red). All remaining parcels are assigned to the warm conveyor belt (green).

baroclinic zone, potential vorticity features from preexisting convection entering a baroclinic zone, shallow baroclinic cyclone formation ahead of a shortwave trough, or tropical cyclone recurvature [Boettcher and Wernli (2013); shown schematically in their Fig. 8]. In all cases, this pattern is represented as an isolated BMF maximum centered on the region of maximum parcel moistening, the favored region for development of lower-level potential vorticity by cloud diabatic heating.

The propagation phase begins following the development of a sufficiently intense circulation, with a maximum positive BMF appearing downshear of the center where the induced flow is oriented perpendicular to the baroclinic zone (Parker and Thorpe 1995). Flow upshear of the center promotes the isentropic downgliding of parcels with their origins in the cooler, drier air mass, combined with those whose specific humidity has been decreased by precipitation fallout in advance of the system. A weak negative BMF feature is, therefore, expected upshear of the vortex center, leading to an asymmetric BMF dipole during this stage of the storm life cycle.

The evolution of a diabatic Rossby vortex in the Atlantic basin in December 2005 provides the opportunity for an evaluation of the conceptual BMF framework for a well-studied event (Boettcher and Wernli 2011).

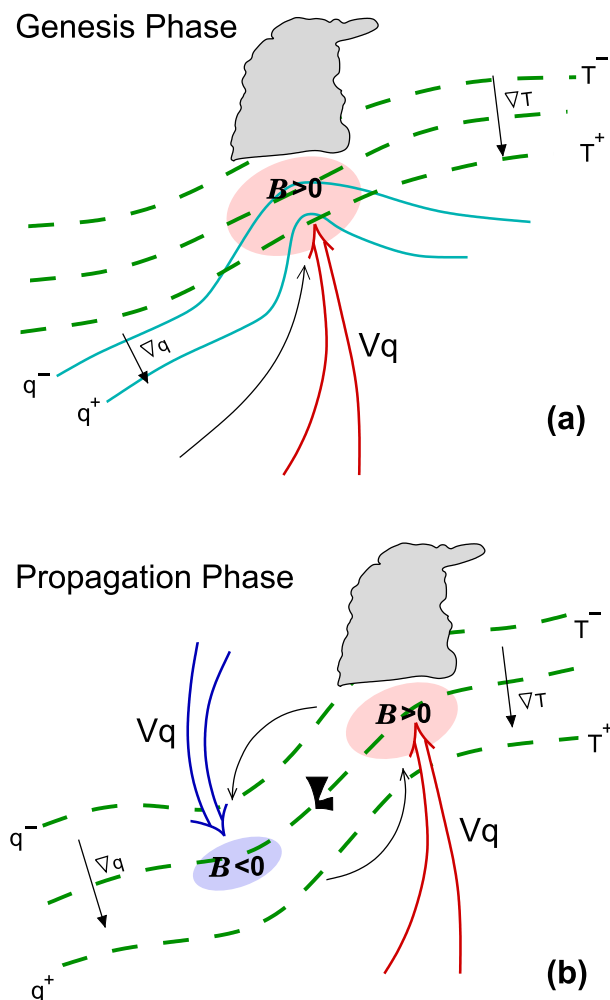## Genesis Phase

Propagation Phase

FIG. 8. Diagram of the conceptual model of the (a) genesis and (b) propagation phases of the diabatic Rossby vortex life cycle. In both panels, isotherms are shown with dashed green lines with the temperature gradient (black arrows with solid heads) oriented toward the bottom right of the plots. Isohumes are plotted with solid cyan contours in (a) and are assumed to be coincident with isotherms in (b). Winds are shown as thin gray lines with open arrow heads, and moisture transports are shown with open arrows (red for poleward transport of moist air and blue for equatorward transport of dry air). Regions where moist diabatic processes are important are represented by a cloudlike symbol, and the position of the low pressure center of the diabatic Rossby vortex is indicated with a black bold somewhat L-looking symbol in (b). Positive and negative extremes of the BMF are shown as pink and light blue shaded regions, respectively, with patch sizes representative of magnitude.

Development occurred over the western Gulf of Mexico on 17 December in the midst of enhanced convective activity facilitated by a southerly surge of warm, moist air across a quasi-stationary baroclinic zone. Moving across the northern Florida peninsula as a mesoscale convective vortex on 18 December, the system encountered enhanced

lower-level baroclinicity associated with the trailing cold front of a synoptic-scale cyclone. The diabatic Rossby vortex entered the propagation phase of its life cycle shortly thereafter, accelerating rapidly east-northeastward along the southern edge of the baroclinic zone. The storm deepened rapidly (36 hPa in 24 h) as an extratropical cyclone in the central North Atlantic on 20 December as it interacted with an approaching upper-level trough. This life cycle is typical of diabatic Rossby vortex-induced explosive cyclogenesis as documented by Wernli et al. (2002).

The structure of the BMF during the genesis phase of the storm's life cycle (Fig. 9a, labeled G) consists of an isolated maximum associated with the isentropic ascent of the southerly flow across the Gulf of Mexico. The time selected for this analysis is 18 h before the initial sea level pressure minimum is identifiable, an indication of the potential predictive capacity of the BMF. Its ability to identify regions in which the process of parcel moistening by isentropic ascent is active focuses attention on areas in which the atmosphere is being preconditioned for moist development before any closed circulation forms. After the onset of the propagation phase of the storm's life cycle (Fig. 9c), the positive BMF maximum shifts to lay downshear of the center as expected based on the conceptual model (Fig. 8b). However, the anticipated negative BMF feature upshear of the low, despite existing as a local minimum in the BMF field, is not sufficiently strong to be apparent in Fig. 9c. This appears to be the result of weak diagnosed isentropic downgliding of very dry air poleward of the baroclinic zone, where precipitable water values are below 15 mm.

While the nascent diabatic Rossby vortex is developing over the Gulf of Mexico, the synoptic steering flow is weak enough ($<$20 kt) that the assumption $\mathbf{C} = 0$ produces a BMF field that is similar to that computed with the best steering estimate (cf. Figs. 9a and 9c). During the propagation phase of the system, however, this value increases to over 40 kt and yields a BMF field that is noticeably different for $\mathbf{C} = 0$ (Fig. 9d). The BMF dipole structure is more evident in the stationary reference frame and is focused more closely on the circulation center as in the conceptual model (Fig. 8b).

A comparison of BMF-relevant structures in the best-estimate and fixed reference frames (Fig. 10) provides an explanation for the sensitivity of the negative component of the BMF field to the synoptic steering flow that generally follows the conceptual model shown in Fig. 2. The steering-relative lower-level circulation of the diabatic Rossby vortex is highly asymmetric at 0000 UTC 20 December 2005, with a strong southerly flow across the baroclinic zone to the east of the center not balanced by a northerly flow of equivalent strength to the west. The presence of ample moisture in the southern section
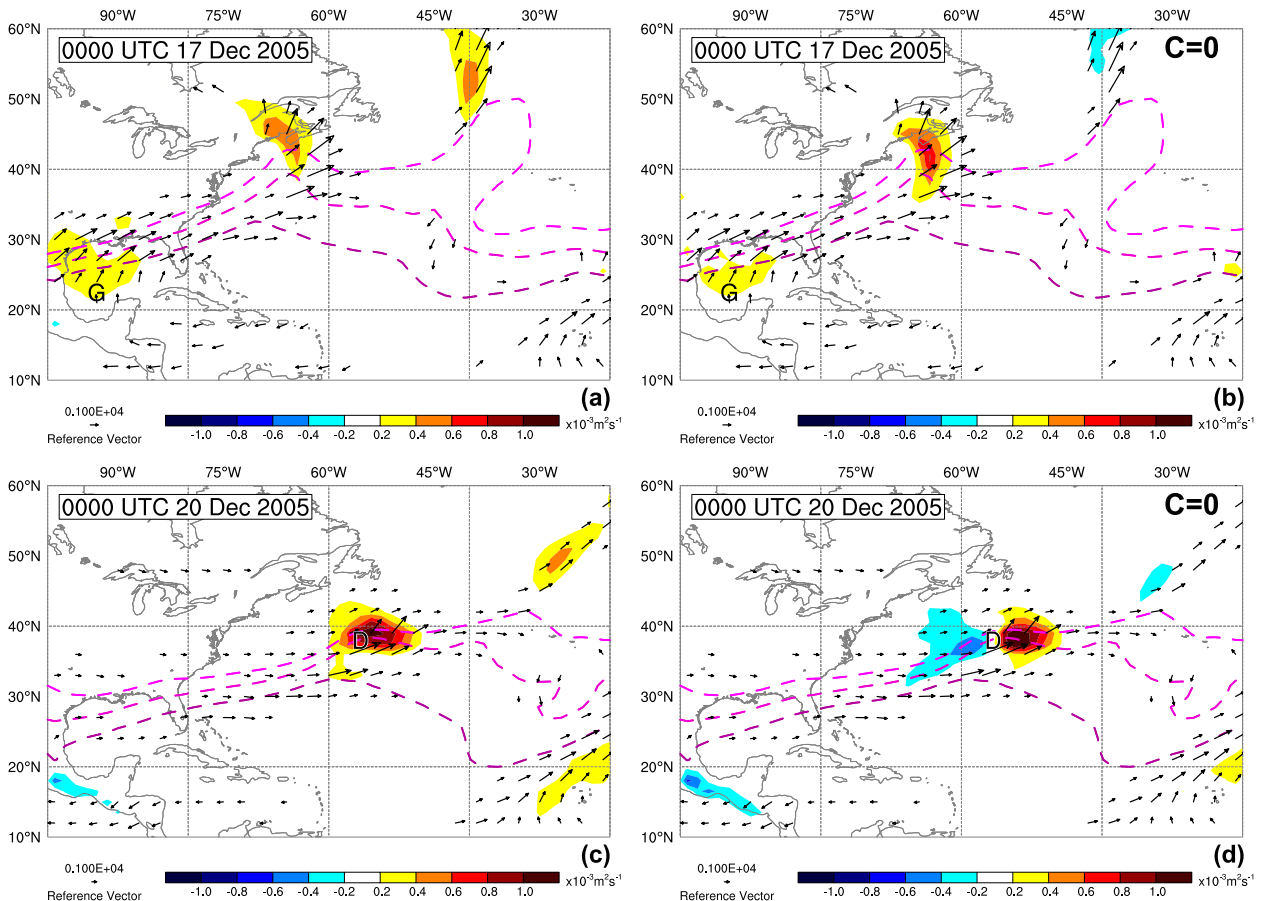
FIG. 9. Free-tropospheric BMF, moisture transport vectors ($\times 10\,\mathrm{kg\,m^{-1}\,s^{-1}}$, see reference vector below each panel), and 1000–500-hPa thickness as in Fig. 5, but for (a),(b) the diabatic Rossby vortex genesis phase at 0000 UTC 17 Dec 2005 and (c),(d) the propagation phase at 0000 UTC 20 Dec 2005. (a),(c) The BMF computed with the best estimate of **C**, and (b),(d) the BMF computed with **C** = 0. The annotation G identifies the location of the nascent diabatic Rossby vortex in (a),(b), and the annotation D indicates the location of the diabatic Rossby vortex low pressure center in (c),(d).

of the system ensures a maximum BMF downshear of the center, where the lower-level flow is perpendicular to both the steering vector and to the baroclinic zone. Upshear however, the lower-level flow closely matches the steering vector, such that parcels appear stationary in the translating reference frame. This yields a null BMF field west of the center in Fig. 10a. In the fixed reference frame, the westerly large-scale flow promotes downgliding across the baroclinic zone in this region, leading to a distinct local minimum in BMF that is focused near the low center because of the elevated moisture content within the circulation (Fig. 10b). The disparity between Fig. 8 and the observed BMF pattern, therefore, appears to follow from the assumption of a symmetric storm-relative lower-level circulation across the baroclinic zone.

Further complication arises from the fact that the observed displacement of the diabatic Rossby vortex (from 246° at 38 kt) has a considerably larger poleward component than suggested by the best estimate of the

synoptic steering flow (from 264° at 40 kt; insensitive to even a 50% increase in the radius for $\mathcal{V}$ to 7.5°). The tendency for diabatic Rossby vortices to cross the baroclinic zone noted by Wernli et al. (2002) may provide an explanation for the enhanced northward displacement of the center. The application of a uniform steering flow (Fig. 11) provides an improved local representation of coherent system displacement, although far-field results are clearly invalid. Under this condition, a region of negative BMF emerges in a pattern reminiscent of the conceptual model (Fig. 8b); however, the northerly lower-level flow that contributes to this structure appears to be more related to the large-scale environment than to the vortex circulation itself. The presence of an identifiable and trackable feature facilitates the definition of such a system velocity for this analysis, but this is not generally possible (e.g., the precirculation genesis phase of this diabatic Rossby vortex). In the current context it is important to note that although the general
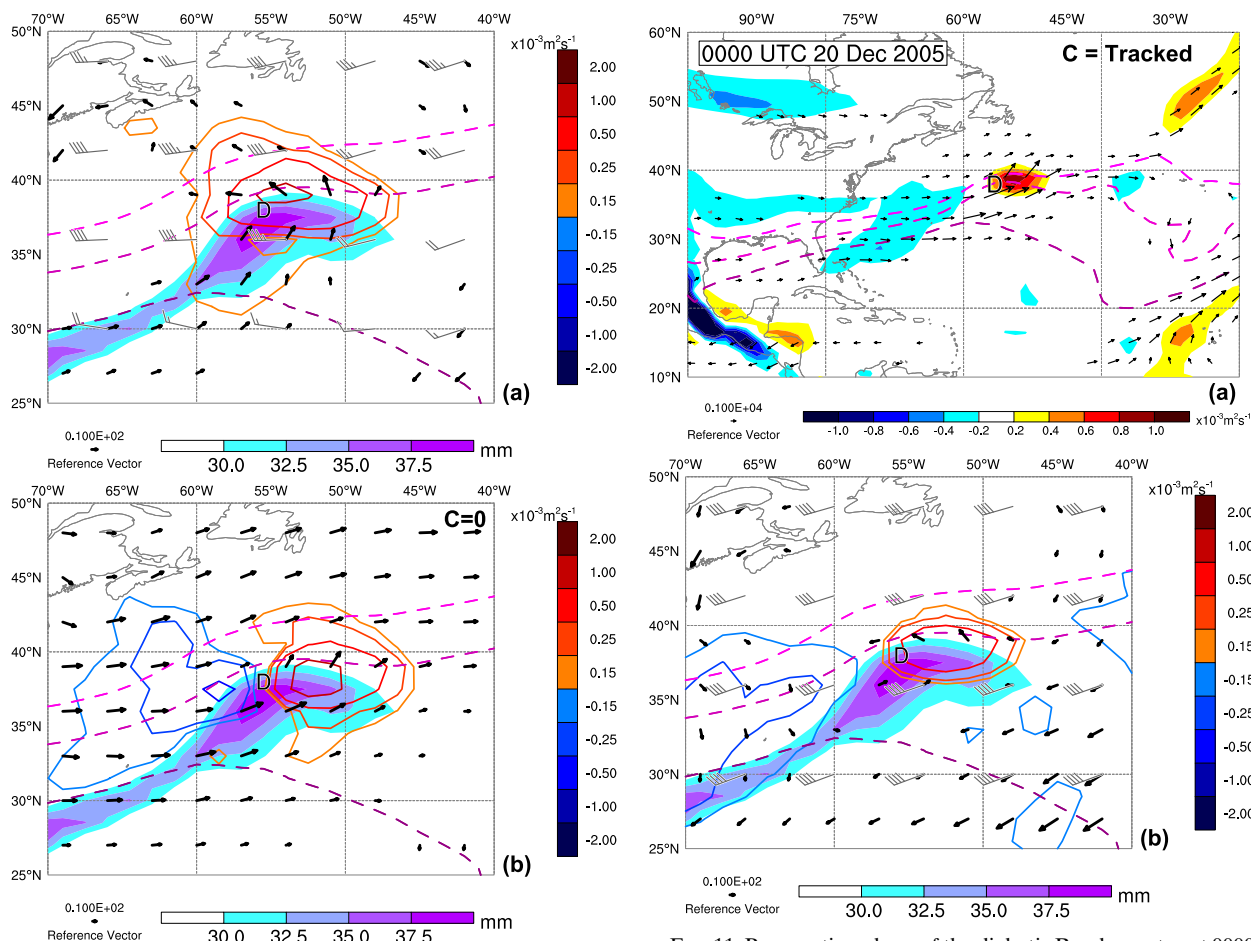
FIG. 10. (a),(b) Analyzed values of precipitable water (mm, color shaded as shown on the horizontal color bar), 1000–500-hPa thickness (dashed contours for 5400, 5520, and 5640 m with lighter magenta colors for smaller thicknesses), synoptic steering flow (gray wind barbs plotted with 5-, 10-, and 50-kt speeds depicted by short long and pennant barbs, respectively), steering-relative mean 850–500-hPa winds (black vectors scaled according to the 10-kt reference vector at the bottom-left corner of the panel, plotted only for speeds above 10 kt), and free-tropospheric BMF (color contours as shown on the vertical color bar). Fields are valid at 0000 UTC 20 Dec 2005, as for Figs. 9c,d. In (a), the best estimate of synoptic steering flow is used for all calculations, while stationary reference frame (**C** = 0) results are shown in (b).
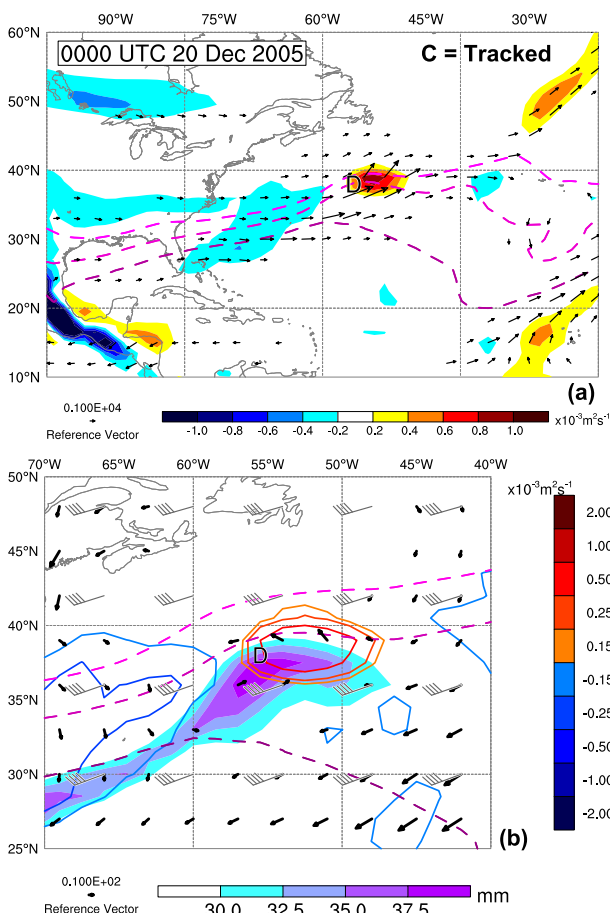

FIG. 11. Propagation phase of the diabatic Rossby vortex at 0000 UTC 20 Dec 2005, with observed system displacement used for the uniform tracked reference frame velocity (from 246° at 38 kt). (a) Plotted as in Fig. 9 and (b) plotted as in Fig. 10.

structure of the BMF maximum is not notably sensitive to **C**, changes to the steering velocity estimate may have noticeable impacts on the details of the BMF signature and negative BMF component of small, fast-moving baroclinic features.

4. Climatological BMF

A 26-yr climatology (1989–2014) of the free-tropospheric BMF [Eq. (12)] is used to evaluate the global relevance of

parcel moistening by isentropic ascent. The properties of the BMF climatology will not necessarily mirror those of any individual feature. Instead, the BMF is expected to highlight simultaneously regions known to favor explosive marine cyclogenesis, moist baroclinic low-level jets, preferred regions for ascent in warm conveyor belts, and other areas in which the isentropic ascent of moist air is prevalent. In addition to describing climatological BMF structures, one of the goals of this section is, therefore, to introduce the links between identifiable BMF patterns and such known atmospheric features in the context of both the best estimate of synoptic steering velocity and **C** = 0. The BMF climatology is described using both mean fields and event counts. The latter are defined as summed instantaneous pointwise exceedances of a threshold BMF value ($\tilde{\mathcal{B}} > 2.5 \times 10^{-4} \, \text{m}^2 \, \text{s}^{-1}$), and provide information about synoptically important transient features whose signatures may not show up clearly in the seasonal mean.
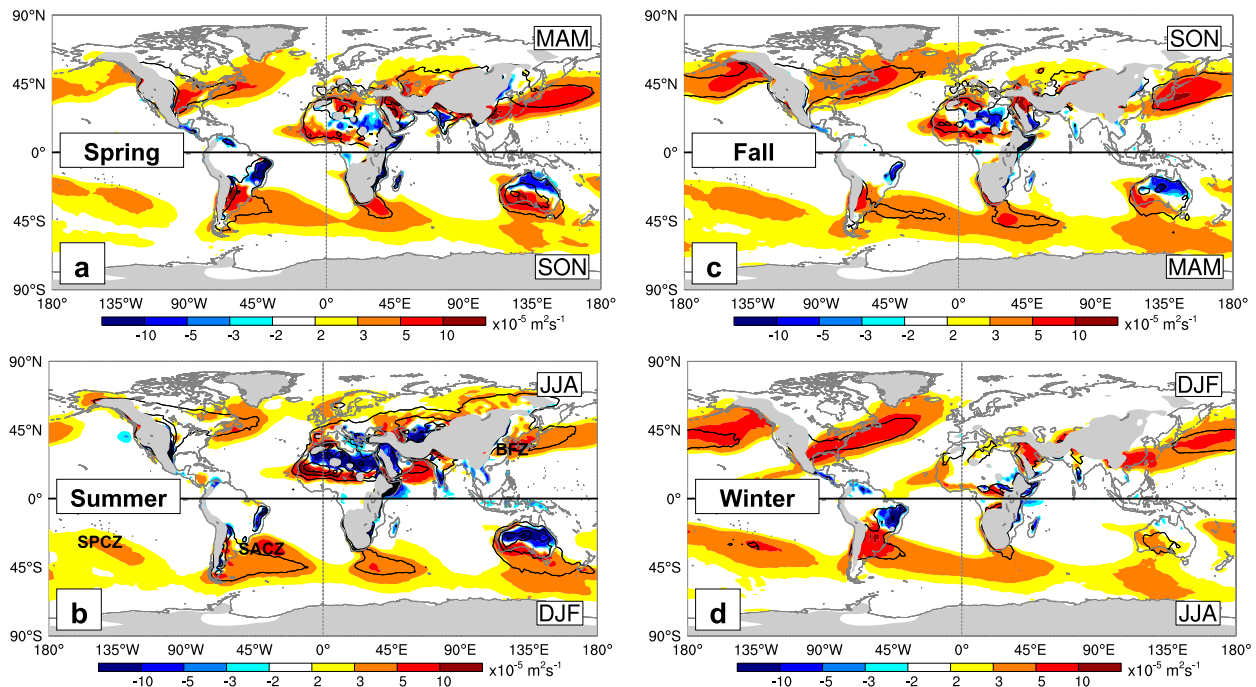
FIG. 12. Mean ($\times 10^{-5}\,\mathrm{m^2\,s^{-1}}$, color shading as indicated on the color bar) and standard deviation (contoured at $15 \times 10^{-5}\,\mathrm{m^2\,s^{-1}}$ intervals) of the free-tropospheric BMF for the hemispheric (a) spring, (b) summer, (c) fall, and (d) winter seasons. Areas with a mean surface pressure < 900 hPa are gray shaded in order to minimize terrain influences on the plotted structures. The approximate positions of the baiu frontal zone (BFZ), South Pacific convergence zone (SPCZ), and South Atlantic convergence zone (SACZ) are provided as annotations in (b).

a. Best estimate of synoptic steering velocity

The global pattern of mean tropospheric BMF is characterized by bands of maxima across the midlatitudes at all seasons (Fig. 12). This pattern is consistent with a Ferrel cell–type description of the Eulerian mean circulation, in which the moist lower-level flow from the subtropics rises as it encounters the polar front (Peixoto and Oort 1992). Frierson et al. (2007) show that such poleward transport of moisture constitutes nearly half of the total energy export to the midlatitudes.

Large BMF variability on both annual and seasonal time scales is found within midlatitude storm tracks (these variabilities are represented by panel-to-panel differences and elevated standard deviation values in Fig. 12, respectively). The high values of the BMF in the winter storm tracks (Fig. 12d) are consistent with the important contribution of synoptic systems to meridional energy transports in a moist isentropic framework (Pauluis et al. 2008). The slantwise neutrality that facilitates these transports (Emanuel 1988) is responsible for both the formation of conveyor belt circulations and the enhanced baroclinic growth rates upon which the synoptic disturbances depend (Sanders and Gyakum 1980; Kuwano-Yoshida and Asuma 2008). The influence

of transient cyclones on mean winter BMF values is evident from the large event counts, particularly in the Northern Hemisphere storm tracks (Fig. 13d). The relative contribution of Southern Hemisphere cyclones to the winter mean midlatitude BMF appears to be smaller: mean BMF values exceed $3 \times 10^{-5}\,\mathrm{m^2\,s^{-1}}$, yet fewer than three events per month are identified in the climatology (Figs. 12d and 13d). This underscores the importance of warm western boundary currents and continental cold air outbreaks to the establishment of strong winter baroclinicity that promotes enhanced isentropic upgliding in the Northern Hemisphere basins (Businger et al. 2005; Yamamoto 2013; Papritz and Spengler 2015).

The zonally elongated BMF patterns of the winter storm tracks give way to isolated maxima over the oceans during the summer (Fig. 12b). Kodama (1992) emphasizes the importance of lower-level moisture transport into the baroclinic "subtropical precipitation zones," including the baiu/mei-yu frontal zone, the South Pacific convergence zone, and the South Atlantic convergence zone (locations noted on Fig. 12b). Upward transport of moisture within the flow impinging on the mean $5\,\mathrm{K}\,(1000\,\mathrm{km})^{-1}$ temperature gradients in these subtropical fronts is noted by Kodama (1992) as a
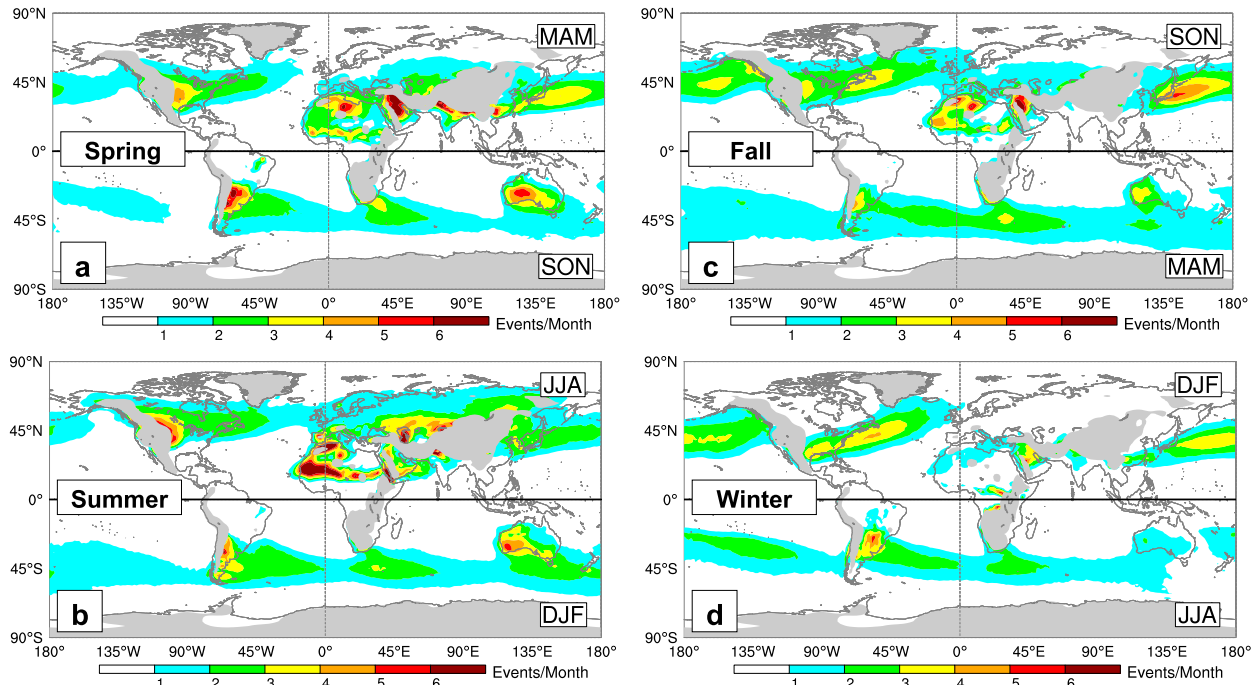
FIG. 13. Monthly frequency (color shading as indicated on the color bar) of large integrated BMF values ($\tilde{\mathcal{B}} > 2.5 \times 10^{-4}\,\mathrm{m^2\,s^{-1}}$) for the hemispheric (a) spring, (b) summer, (c) fall, and (d) winter seasons. Areas with a mean surface pressure < 900 hPa are gray shaded in order to minimize terrain influences on the plotted structures.

thermodynamically important characteristic of these features (his Fig. 16). The quasi-steady nature of these features is highlighted by the lack of large BMF events in these regions (Fig. 13b).

The largest mean oceanic BMF values and event counts are found in the western North Pacific basin in the fall season (Figs. 12c and 13c), consistent with the prevalence of tropical cyclones recurving into the baroclinic westerlies in the region (Klein et al. 2000; Archambault et al. 2013). Air parcels of tropical origin ascend sloping isentropes ahead of these storms as they approach the midlatitude baroclinic zone prior to extratropical transition (Jones et al. 2003), potentially leading to the formation of predecessor rain events (Galarneau et al. 2010). During extratropical transition, isentropic upgliding is essential for moistening parcels near the remnant core and in the developing warm conveyor belt circulations, yielding peak BMF values during these events (Grams et al. 2011). Archambault et al. (2013) find that, on average, five recurvature events occur each fall in the western North Pacific basin, such that at least one-third of the large BMF event maximum shown in Fig. 13c is likely to be directly associated with transitioning tropical cyclones or attendant predecessor rain events.

The impact of atmospheric rivers and tropical moisture exports on the BMF climatology is apparent in the fall and winter seasons as an eastward extension of high

BMF values and relatively large event counts into the eastern peripheries of the ocean basins (Figs. 12c,d and 13c,d). These regions are coincident with those of maximum winter meridional moisture transport identified by Zhu and Newell (1998), consistent with the ascent of air parcels of subtropical origin along the sloping isentropes of the midlatitude baroclinic zones. The transient nature of atmospheric rivers suggests that the large BMF events in these regions are likely associated with enhanced ascent in the warm conveyor belts of baroclinic cyclones of the type discussed in section 3a, rather than background meridional circulations. Selecting the months of peak hemispheric warm conveyor belt mass fluxes identified by Eckhardt et al. (2004), the global distribution of large BMF event counts matches closely with that of precipitation associated with warm conveyor belt trajectories (Fig. 14). This suggests that isentropic ascent in warm conveyor belts is a dominant process for parcel moistening, cloud, and precipitation formation on a global scale throughout the cold season (Pfahl et al. 2014).

Despite the weakening and poleward retreat of the midlatitude baroclinic zones in summer, diabatic Rossby vortex activity reaches its peak in the warm season (Boettcher and Wernli 2013, 2015). The zonal alignment of the axis of summer BMF events in the North Atlantic and North Pacific basins (Fig. 13b) is consistent with
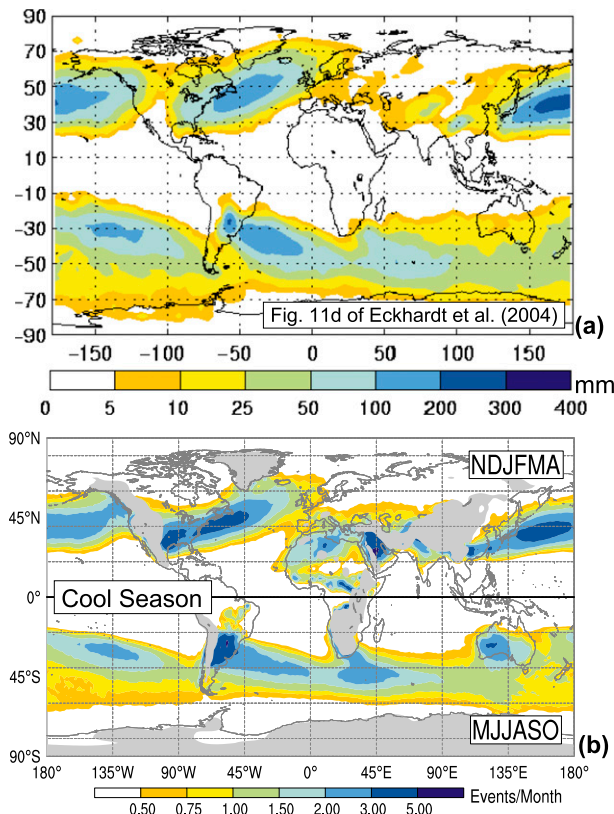
FIG. 14. (a) Annual warm conveyor belt-related precipitation totals, reproduced from Eckhardt et al. (2004) for reference (©American Meteorological Society, used with permission). (b) The monthly frequency of large integrated BMF values is shown for the cold season in each hemisphere (November–April in the Northern Hemisphere and May–October in the Southern Hemisphere). These are the periods during which warm conveyor belts are most active and constitute leading contributors to oceanic BMF. Although they represent distinct quantities, color scales are matched between the panels to ease comparison.

diabatic Rossby vortex track direction. However, the relatively low frequency (less than one event per month even in the high-density development regions near the western boundaries of the basins), small spatial scale, and generally weak intensity of warm-season diabatic Rossby vortices suggests that they are likely secondary contributors to the overall BMF event count. A more refined stratification procedure would be needed to isolate the contribution of diabatic Rossby vortices to the seasonal BMF, especially later in the warm season when recurving tropical cyclones (some of which spawn diabatic Rossby vortices) dominate the climatology as discussed above.

Although the distribution of BMF over land is highly variable in both space and time, the largest absolute values occur during the summer over the tropical and subtropical continents (Fig. 12b) in association with monsoon and low-level jet circulations. These features

are most prominent over North Africa and Australia, two regions whose summer circulation patterns are dominated by heat lows and relatively cool adjacent waters (Sultan and Janicot 2003; Manton and McBride 1992). These areas are considered in more detail in the appendix to ensure that the large amplitudes and variabilities of the BMF fields therein are reliable indications of episodic parcel moistening by isentropic ascent, and are not spurious patterns resulting from the prevalence strong diabatic heating and diurnal cycles. This analysis highlights the ability of the BMF to serve as an exploratory diagnostic: large land-based values were not expected at the outset of this investigation, but are shown in the appendix to be related to relatively moist parcels undergoing isentropic ascent and impacting sensible weather in these regions.

b. Stationary reference frame

The adoption of a stationary reference frame ($\mathbf{C} = 0$) for the calculation of the BMF has the advantage of computational simplicity and may arguably be more relevant in regions where circulations are linked to topography as discussed in section 3a. However, this simplifying assumption has a dramatic impact on the seasonal mean oceanic BMF structure in areas where mobile cyclones dominate the climatology (cf. Figs. 12 and 15). The elevated BMF values ascribed to the midlatitude storm tracks in the previous section are dramatically reduced when this form of the diagnostic is employed; however, the increased BMF standard deviation in these regions is indicative of the explanation for this change in structure. When the stationary reference frame is adopted for midlatitude cyclones, larger negative values of the BMF appear as described in section 2a (Fig. 2). This increases variability but decreases the mean BMF values dramatically in regions where such systems are prevalent. This interpretation of the source of changes in the mean BMF is consistent with the relative insensitivity of the BMF event count to the change in reference frame (cf. Figs. 13 and 16), because the latter depends uniquely on the frequency of large positive BMF values.

Both the mean and the event BMF climatologies over land are relatively insensitive to the adoption of the stationary reference frame, a finding that underscores the importance of geography in anchoring the circulations responsible for the local BMF patterns. The monsoon and low-level jet-related continental BMF extremes in the summer season are generally unaffected by the adoption of $\mathbf{C} = 0$, although the spring–summer maximum in BMF events over the Great Plains of North America is more evident in this framework. Trier et al. (2006) show that isentropic ascent of the southerly
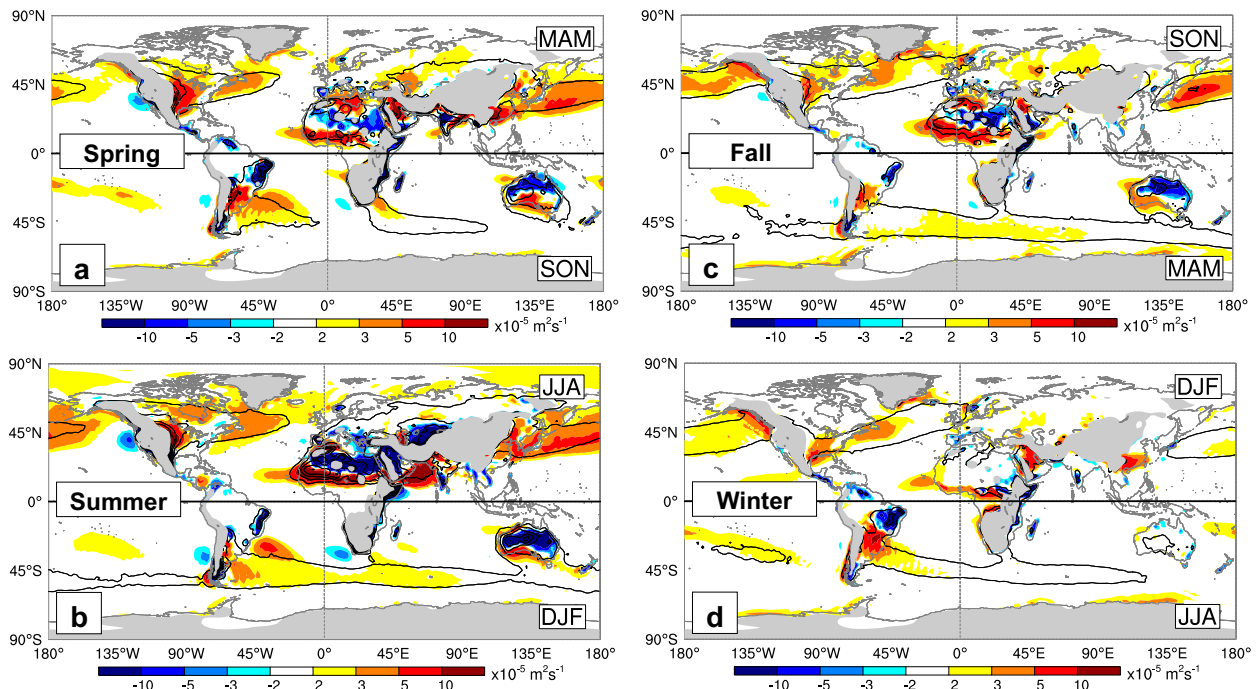
FIG. 15. As in Fig. 12, but for a stationary reference frame ($\mathbf{C} = 0$).

nocturnal jet in this region leads to moistening at the top of the boundary layer that supports the development and maintenance of mesoscale convective systems. The BMF mean and event maxima that lie along the west coasts of North America and northern Europe in the fall and winter seasons are more pronounced in the stationary reference frame as expected for terrain-influenced baroclinicity and associated ascent (section 3a). Because these are the preferred regions for extreme precipitation related to landfalling atmospheric rivers, these large-amplitude BMF maxima represent an important manifestation of the process of parcel moistening by isentropic ascent.

The validity of the adoption of the stationary reference frame, therefore, depends on both the class of feature and the metric selected for investigation. The inclusion of an appropriate synoptic phase speed is highly relevant for fast-moving, oceanic features, unless only positive BMF events are of concern. However, the use of $\mathbf{C} = 0$ is defensible for topographically anchored circulations for both climatological means and event counts.

5. Summary and discussion

The primary goal of this study has been to develop a diagnostic quantity that highlights the process of parcel moistening by isentropic ascent. This process is highly relevant for an important class of synoptic and mesoscale systems that derive much of the energy for their circulation from the release of latent heat. The BMF is able to identify systems in which isentropic upgliding is bringing parcels toward saturation, in addition to highlighting regions in which the process itself is active without any a priori knowledge of the type of weather systems involved. The BMF can, therefore, act as either a filtering or an exploratory quantity because of its process-centric formulation. This distinguishes the BMF from other diagnostics that relate moisture, clouds, and precipitation fields such as the moisture flux convergence. Large values of the latter may be indicative of regions in which moisture is accumulating, but they do little to describe the process by which this moistening is occurring. In addition to identifying regions favorable to the development of active weather, the BMF provides important information about the dynamical nature of the circulation involved.

The vertical moisture flux forms the basis for the BMF because of its direct relevance to parcel moistening from a Lagrangian perspective. To focus only on ascent along sloping isentropic surfaces, the full vertical motion field is replaced with the isentropic upglide component as defined by Hoskins et al. (2003). As for isentropic analysis in general, the calculation of this quantity relies on the estimation of a synoptic steering velocity that corresponds to the translation of the reference frame in which the circulation is considered. The optimal
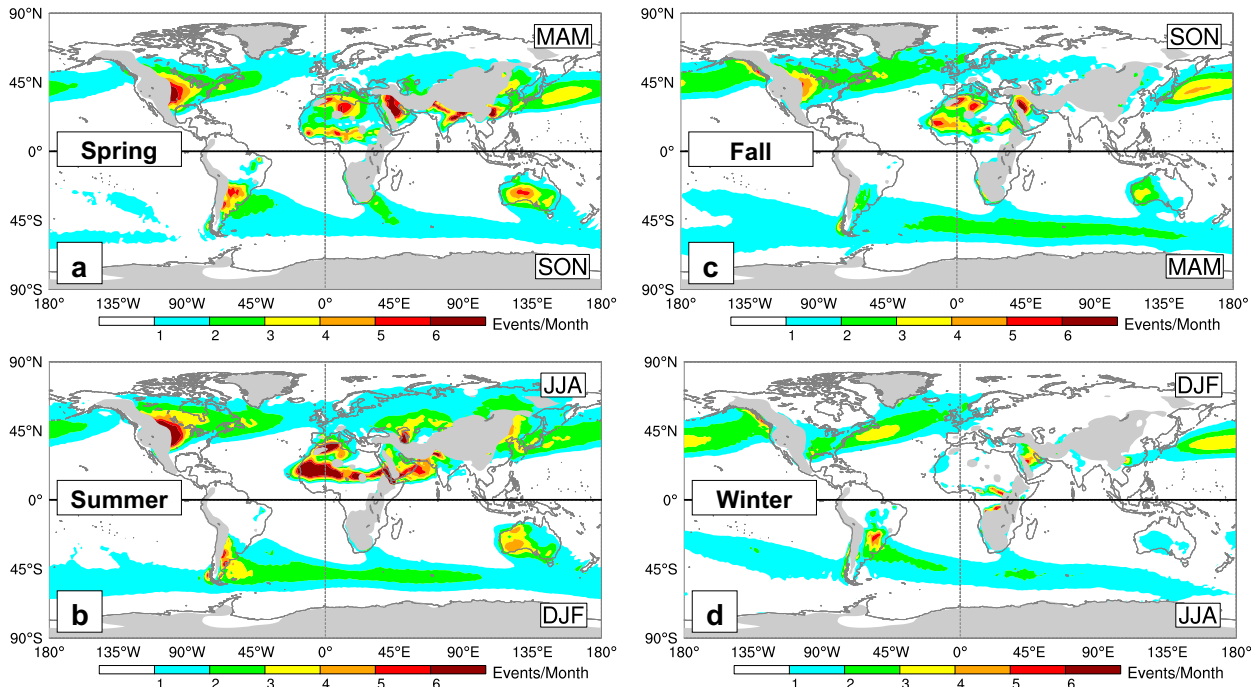
FIG. 16. As in Fig. 13, but for a stationary reference frame (**C** = 0).

synoptic steering velocity is determined through the minimization of the isentropic displacement component of vertical motion relative to isentropic upgliding. In theory, this method yields the best estimate of the steering flow; however, the computationally complex technique requires the prescription of a system size and access to comprehensive three-dimensional data for volume integrals. These factors may make its application difficult in the context of limited data or computational resources. The impact of adopting a simplified stationary reference frame has also been investigated, and shown to be a justifiable approximation when thermal gradients are anchored to orography and, therefore, do not move with the synoptic flow. A more detailed analysis of alternative steering flow estimates to be undertaken in a follow-up study should yield additional guidance on this subject for future research involving the BMF.

A pair of case studies serves to document the characteristics of the BMF for canonical systems in which the process of parcel moistening by isentropic ascent is known to be of leading-order importance. An axis of elevated integrated vapor transport extends from the subtropical Atlantic to the coast of Norway, but the bulk of precipitation is focused in the head region of the circulation as parcels ascent rapidly across the warm frontal zone, a region of peak BMF. The life cycle stages of a diabatic Rossby vortex appear to be associated with

changes in the structure of the BMF associated with the system. An initial positive monopole evolves into a BMF dipole as the vortex enters the propagation phase, and, thereafter, relaxes back toward an isolated maximum as the storm undergoes seclusion (final stage not shown). Although the range of features investigated is necessarily limited, these cases illustrate the physical relevance of the BMF to systems for which parcel moistening by isentropic ascent is essential.

The climatological distribution of the BMF highlights regions in which moistening by isentropic upgliding is active on a broad range of scales. Poleward latent heat transports by the Eulerian mean flow are seasonally modulated by enhanced BMF values along the oceanic storm tracks and in subtropical precipitation zones. Over land the structure of the BMF climatology is more complex, with direct links to seasonal monsoon circulations and low-level jets. Analysis of the dominant features present in the climatology suggests that the diagnostic effectively identifies regions in which circulations known to involve the isentropic upgliding of moist air are active. From an exploratory perspective, other climatological BMF structures have not been associated with well-documented flows in this investigation [e.g., persistent large mean BMF values over western Russia and the Arabian peninsula, the latter having just recently received the attention of de Vries et al. (2016)] and may, therefore, be worthy of additional study.

The BMF appears to successfully identify regions in which parcels are being moistened by isentropic upgliding; however, once condensation begins the vertical motion of the parcel changes dramatically as it begins to ascend the moist isentrope. This transition from adiabatic to moist ascent is not explicitly represented in the form of the BMF developed in section 2 because of the use of the dry static stability in Eq. (11). Although the current formulation remains qualitatively valid during moist ascent, the incorporation of an effective stability that accounts for the influences of fractional cloudiness in subsaturated environments (O'Gorman 2011) will increase positive BMF values in moist ascending airstreams. This extension of the BMF will be the subject of a future study, though preliminary analyses suggest that climatological event counts are generally consistent with those shown here for an equivalent detection threshold.

The process-oriented foundation of the BMF makes it a potentially useful quantity for a broad range of applications. The filtering properties of the diagnostic could be employed in objective cyclone identification to discriminate between systems for which parcel moistening by isentropic ascent has a primary or secondary impact on the circulation. It may be useful for weather and climate model diagnosis and evaluation, especially given expected changes in the moisture content of a warmer climate (Held and Soden 2006). The proposal of a simplified estimate of the synoptic steering velocity will be particularly useful in the climate modeling context because of typically limited data availability. The possibility that the BMF possesses a predictive capacity has not been explored in this study. However, as noted for the diabatic Rossby vortex case study (section 3b), the fact that parcel moistening by isentropic ascent preceded the formation of any closed circulation suggests that the BMF may be capable of identifying regions in which this process is actively preconditioning an environment for storm formation. In aggregate, these attributes of the BMF suggest that it may be valuable in a broad range of contexts as a physically relevant, process-driven diagnostic quantity.

APPENDIX

Exploratory Analysis: Continental BMF Extremes

The northwest African summer environment is dominated by the West African monsoon, a complex feature rooted in the presence of the Saharan heat low at 25°–30°N and the Atlantic cold tongue in the Gulf of Guinea (Okumura and Xie 2004) that combine to give rise to the African easterly jet. The anticyclonic heat-low outflow at 700 hPa (centered near the prime meridian) promotes northerly and northeasterly midlevel winds across the Sahara and into the confluent jet entrance region. Despite the generally low moisture content of this circulation, strong isentropic downgliding as the parcels approach the heat low yields large negative BMF values (Fig. 12b). This mean flow is punctuated by outbreaks of more humid air from the Mediterranean (Nieto et al. 2006), which penetrate southward and cause localized increases in the amplitude of the negative BMF. To the south of the heat-low center, the mean meridional flow is described by a pair of overturning circulations: a deep cell associated with the intertropical convergence zone, and a shallow one related to low-level thermal gradients and dry convection over the desert [conceptual schematic shown in Fig. 12 of Thorncroft et al. (2011)]. Moisture transports across the Sahel (Salih et al. 2015) are complicated by the presence of strong diurnal variability in which cool, moist air surges northward at very low levels overnight (below 900 hPa), is mixed vertically by dry convection in the deep Saharan boundary layer during the day, and then moves southward in a return flow centered at 700 hPa (Parker et al. 2005; Thorncroft et al. 2011). The 850–250-hPa-integrated BMF represents only the upper portion of this cell, in which the northerly flow ascends the sloping isentropes of the intertropical front (Lélé and Lamb 2010). Parcel

moistening by isentropic ascent in this circulation may help to limit evaporative downdraft formation as these parcels are ingested into the intertropical convergence zone over the Sahel. In the northwest African summer, the integrated BMF, therefore, appears to be highlighting physically relevant circulations that are directly related to sensible weather across the region.

The Australian monsoon is part of a larger summer system that exists over the Maritime Continent (McBride 1998), although the flow over much of Australia is dominated by the presence of a heat low over the Great Sandy Desert [near 20°S and 125°W; Wheeler and McBride (2005)]. Despite large variability on intraseasonal, synoptic, and diurnal time scales (Troup 1961; Hanstrum et al. 1990; Berry et al. 2011), the characteristics of the circulation and moisture fluxes associated with the Australian heat low are broadly similar to those of its Saharan counterpart (Spengler et al. 2005). Easterly flow across the central continent at lower levels becomes southerly in the shallow anticyclonic heat-low outflow at 700 hPa, leading to the equatorward advection of relatively cool air and the formation of a thermal trough over eastern Australia. The implied isentropic downgliding combines with the formation of a deep mixed layer in the late afternoon that effectively moistens the 700-hPa flow, yielding large negative BMF values over the central and northern parts of the continent. At the same time, cool, moist air is transported northward across the southern coast by the low-level inflow of the heat low (below 900 hPa). As in the Sahel, mixing and return flow processes yield a region of positive 850–250-hPa-integrated BMF values in this meridional circulation cell.

Despite the similarity of the heat low dynamics of the West African and Australian monsoons, the correlation between their associated BMF structures regional precipitation patterns is dramatically different. Over North Africa, parcel moistening by isentropic upgliding appears to be assisting with the formation of clouds and precipitation. In the Australian summer, however, peak rainfall totals are concentrated in the extreme northern section of the continent where BMF values are small. At least part of this contrast may be explained by the difference in meridional temperature gradients equatorward of the heat low. There is no Australian analog to the Atlantic cold tongue that plays such an important role over the Sahel; instead, the waters across the Maritime Continent remain warm throughout the summer (Waliser 1996) and, therefore, support little background baroclinicity. Complicating this interpretation is the presence of strong diurnal cycles of diabatic heating in these regions, the direct effect of which is to deform isentropic surfaces and thus amplify ω_{ID}; however, the climatological value of Γ in these areas remains well below unity (Fig. 3b), implying that the impact of this process is secondary. Although this analysis suggests that the BMF is highlighting physically relevant structures, further analysis of the relative importance of parcel moistening by isentropic ascent in monsoon circulations in general may yield additional insight into both the behavior of the BMF and the underlying dynamics active in these regions.

REFERENCES

Archambault, H. M., L. F. Bosart, and J. M. Cordeira, 2013: A climatological analysis of the extratropical flow response to recurving western North Pacific tropical cyclones. *Mon. Wea. Rev.*, **141**, 2325–2346, doi:10.1175/MWR-D-12-00257.1.

Benton, G. S., and M. A. Estoque, 1954: Water-vapor transfer over the North American continent. *J. Meteor.*, **11**, 462–477, doi:10.1175/1520-0469(1954)011<0462:WVTOTN>2.0.CO;2.

Berry, G., M. J. Reeder, and C. Jakob, 2011: Physical mechanisms regulating summertime rainfall over northwestern Australia. *J. Climate*, **24**, 3705–3717, doi:10.1175/2011JCLI3943.1.

Boettcher, M., and H. Wernli, 2011: Life cycle study of a diabatic Rossby wave as a precursor to rapid cyclogenesis in the North Atlantic—Dynamics and forecast performance. *Mon. Wea. Rev.*, **139**, 1861–1878, doi:10.1175/2011MWR3504.1.

——, and ——, 2013: A 10-yr climatology of diabatic Rossby waves in the Northern Hemisphere. *Mon. Wea. Rev.*, **141**, 1139–1154, doi:10.1175/MWR-D-12-00012.1.

——, and ——, 2015: Diabatic Rossby waves in the Southern Hemisphere. *Quart. J. Roy. Meteor. Soc.*, **141**, 3106–3117, doi:10.1002/qj.2595.

Boos, W. R., and K. A. Emanuel, 2009: Annual intensification of the Somali jet in a quasi-equilibrium framework: Observational composites. *Quart. J. Roy. Meteor. Soc.*, **135**, 319–335, doi:10.1002/qj.388.

Bosart, J. L., 1981: The President's Day snowstorm of 18–19 February 1979: A subsynoptic-scale event. *Mon. Wea. Rev.*, **109**, 1542–1566, doi:10.1175/1520-0493(1981)109<1542:TPDSOF>2.0.CO;2.

Browning, K. A., 1985: Conceptual models of precipitation systems. *Meteor. Mag.*, **114**, 293–319.

——, 1990: Organization of clouds and precipitation in extratropical cyclones. *Extratropical Cyclones: The Erik H. Palmén Memorial Volume*, C. Newton and E. Holopainen, Eds., Amer. Meteor. Soc., 129–153.

——, and N. M. Roberts, 1994: Structure of a frontal cyclone. *Quart. J. Roy. Meteor. Soc.*, **120**, 1535–1557, doi:10.1002/qj.49712052006.

Businger, S., T. M. Graziano, M. L. Kaplan, and R. A. Rozumalski, 2005: Cold-air cyclogenesis along the Gulf-Stream front: Investigation of diabatic impacts on cyclone development, frontal structure, and track. *Meteor. Atmos. Phys.*, **88**, 65–90, doi:10.1007/s00703-003-0050-y.

Carlson, T. N., 1980: Airflow through midlatitude cyclones and the comma cloud pattern. *Mon. Wea. Rev.*, **108**, 1498–1509, doi:10.1175/1520-0493(1980)108<1498:ATMCAT>2.0.CO;2.

Carroll, E. B., 2003: Thermal advection, vorticity advection and potential vorticity advection in extra-tropical synoptic-scale development. *Meteor. Appl.*, **10**, 281–292, doi:10.1017/S1350482703003086.

Cook, K. H., 1999: Generation of the African easterly jet and its role in determining West African precipitation. *J. Climate*, **12**, 1165–1184, doi:10.1175/1520-0442(1999)012<1165:GOTAEJ>2.0.CO;2.

Davis, C. A., and L. F. Bosart, 2003: Baroclinically induced tropical cyclogenesis. *Mon. Wea. Rev.*, **131**, 2730–2747, doi:10.1175/1520-0493(2003)131<2730:BITC>2.0.CO;2.

de Vries, A. J., S. B. Feldstein, E. Tyrlis, M. Riemer, M. Baumgart, M. Fnais, M. Sprenger, and J. Lelieveld, 2016: Dynamics of tropical-extratropical interactions and extreme precipitation events in Saudi Arabia in autumn, winter and spring. *Quart. J. Roy. Meteor. Soc.*, **142**, 1862–1880, doi:10.1002/qj.2781.

Dee, D. P., and Coauthors, 2011: The ERA-Interim reanalysis: Configuration and performance of the data assimilation system. *Quart. J. Roy. Meteor. Soc.*, **137**, 553–597, doi:10.1002/qj.828.

Eckhardt, S., A. Stohl, H. Wernli, P. James, C. Forster, and N. Spichtinger, 2004: A 15-year climatology of warm conveyor belts. *J. Climate*, **17**, 218–237, doi:10.1175/1520-0442(2004)017<0218:AYCOWC>2.0.CO;2.

Emanuel, K. A., 1988: Observational evidence of slantwise convective adjustment. *Mon. Wea. Rev.*, **116**, 1805–1816, doi:10.1175/1520-0493(1988)116<1805:OEOSCA>2.0.CO;2.

——, 2005: Genesis and maintenance of "Mediterranean hurricanes." *Adv. Geosci.*, **2**, 217–220, doi:10.5194/adgeo-2-217-2005.

Evans, C., and R. E. Hart, 2008: Analysis of the wind field evolution associated with the extratropical transition of Bonnie (1998). *Mon. Wea. Rev.*, **136**, 2047–2065, doi:10.1175/2007MWR2051.1.

Frierson, D. M. W., I. M. Held, and P. Zurita-Gotor, 2007: A gray-radiation aquaplanet moist GCM. Part II: Energy transports in altered climates. *J. Atmos. Sci.*, **64**, 1680–1693, doi:10.1175/JAS3913.1.

Galarneau, T. J., Jr., L. F. Bosart, and R. S. Schumacher, 2010: Predecessor rain events ahead of tropical cyclones. *Mon. Wea. Rev.*, **138**, 3272–3297, doi:10.1175/2010MWR3243.1.

Grams, C. M., and Coauthors, 2011: The key role of diabatic processes in modifying the upper-tropospheric wave guide: A North Atlantic case-study. *Quart. J. Roy. Meteor. Soc.*, **137**, 2174–2193, doi:10.1002/qj.891.

Green, J. S. A., F. H. Ludlam, and J. F. R. McIlveen, 1966: Isentropic relative-flow analysis and the parcel theory. *Quart. J. Roy. Meteor. Soc.*, **92**, 210–219, doi:10.1002/qj.49709239204.

Grotjahn, R., and C.-H. Wang, 1989: On the source of air modified by ocean surface fluxes to enhance frontal cyclone development. *Ocean–Air Interact.*, **1**, 257–288.

Hanstrum, B. N., K. J. Wilson, and S. L. Barrell, 1990: Prefrontal troughs over southern Australia. Part I: A climatology. *Wea. Forecasting*, **5**, 22–31, doi:10.1175/1520-0434(1990)005<0022:PTOSAP>2.0.CO;2.

Held, I. M., and B. J. Soden, 2006: Robust responses of the hydrological cycle to global warming. *J. Climate*, **19**, 5686–5699, doi:10.1175/JCLI3990.1.

——, R. L. Panetta, and R. T. Pierrehumbert, 1985: Stationary external Rossby waves in vertical shear. *J. Atmos. Sci.*, **42**, 865–883, doi:10.1175/1520-0469(1985)042<0865:SERWIV>2.0.CO;2.

Hennon, C. C., and Coauthors, 2013: Tropical cloud cluster climatology, variability, and genesis productivity. *J. Climate*, **26**, 3046–3066, doi:10.1175/JCLI-D-12-00387.1.

Higgins, R. W., Y. Yao, E. S. Yarosh, J. E. Janowiak, and K. C. Mo, 1997: Influence of the Great Plains low-level jet on summertime precipitation and moisture transport over the central United States. *J. Climate*, **10**, 481–507, doi:10.1175/1520-0442(1997)010<0481:IOTGPL>2.0.CO;2.

Hirata, H., R. Kawamura, M. Kato, and T. Shinoda, 2015: Influential role of moisture supply from the Kuroshio/Kuroshio Extension in the rapid development of an extratropical cyclone. *Mon. Wea. Rev.*, **143**, 4126–4144, doi:10.1175/MWR-D-15-0016.1.

Hoskins, B., M. Pedder, and D. Wyn Jones, 2003: The omega equation and potential vorticity. *Quart. J. Roy. Meteor. Soc.*, **129**, 3277–3303, doi:10.1256/qj.02.135.

Jones, S. C., and Coauthors, 2003: The extratropical transition of tropical cyclones: Forecast challenges, current understanding, and future directions. *Wea. Forecasting*, **18**, 1052–1092, doi:10.1175/1520-0434(2003)018<1052:TETOTC>2.0.CO;2.

Kain, J. S., S. M. Goss, and M. E. Baldwin, 2000: The melting effect as a factor in precipitation-type forecasting. *Wea. Forecasting*, **15**, 700–714, doi:10.1175/1520-0434(2000)015<0700:TMEAAF>2.0.CO;2.

Klein, P. M., P. A. Harr, and R. L. Elsberry, 2000: Extratropical transition of western North Pacific tropical cyclones: An overview and conceptual model of the transformation stage. *Wea. Forecasting*, **15**, 373–395, doi:10.1175/1520-0434(2000)015<0373:ETOWNP>2.0.CO;2.

Knippertz, P., and H. Wernli, 2010: A Lagrangian climatology of tropical moisture exports to the Northern Hemisphere extratropics. *J. Climate*, **23**, 987–1003, doi:10.1175/2009JCLI3333.1.

——, ——, and G. Gläser, 2013: A global climatology of tropical moisture exports. *J. Climate*, **26**, 3031–3045, doi:10.1175/JCLI-D-12-00401.1.

Kodama, Y., 1992: Large-scale common features of subtropical precipitation zones (the Baiu frontal zone, the SPCZ, and the SACZ). Part I: Characteristics of subtropical frontal zones. *J. Meteor. Soc. Japan*, **70**, 813–835.

Korolev, A. V., and I. P. Maxin, 2003: Supersaturation of water vapor in clouds. *J. Atmos. Sci.*, **60**, 2957–2974, doi:10.1175/1520-0469(2003)060<2957:SOWVIC>2.0.CO;2.

Kuo, Y.-H., M. A. Shapiro, and E. G. Donall, 1991: The interaction between baroclinic and diabatic processes in a numerical simulation of a rapidly intensifying extratropical marine cyclone. *Mon. Wea. Rev.*, **119**, 368–384, doi:10.1175/1520-0493(1991)119<0368:TIBBAD>2.0.CO;2.

Kuwano-Yoshida, A., and Y. Asuma, 2008: Numerical study of explosively developing extratropical cyclones in the Northwestern Pacific region. *Mon. Wea. Rev.*, **136**, 712–740, doi:10.1175/2007MWR2111.1.

Lackmann, G. M., D. Keyser, and L. F. Bosart, 1999: Energetics of an intensifying jet streak during the experiment on rapidly intensifying cyclones over the Atlantic (ERICA). *Mon. Wea. Rev.*, **127**, 2777–2795, doi:10.1175/1520-0493(1999)127<2777:EOAIJS>2.0.CO;2.

Larson, V. E., R. Wood, P. R. Field, J.-C. Golaz, T. H. Vonder Harr, and W. R. Cotton, 2001: Small-scale and mesoscale variability of scalars in cloudy boundary layers: One-dimensional probability density functions. *J. Atmos. Sci.*, **58**, 1978–1994, doi:10.1175/1520-0469(2001)058<1978:SSAMVO>2.0.CO;2.

Lavers, D. A., R. P. Allan, E. F. Wood, G. Villarini, D. J. Brayshaw, and A. J. Wade, 2011: Winter floods in Britain are connected to atmospheric rivers. *Geophys. Res. Lett.*, **38**, L23803, doi:10.1029/2011GL049783.

Lélé, M. I., and P. J. Lamb, 2010: Variability of the intertropical front (ITF) and rainfall over the West African Sudan–Sahel zone. *J. Climate*, **23**, 3984–4004, doi:10.1175/2010JCLI3277.1.

Madonna, E., H. Wernli, and H. Joos, 2014: Warm conveyor belts in the ERA-Interim dataset (1979–2010). Part I: Climatology and potential vorticity evolution. *J. Climate*, **27**, 3–26, doi:10.1175/JCLI-D-12-00720.1.

Manton, M. J., and J. L. McBride, 1992: Recent research on the Australian monsoon. *J. Meteor. Soc. Japan*, **70**, 275–285.

McBride, J., 1998: Indonesia, Papua New Guinea, and tropical Australia: The Southern Hemisphere monsoon. *Meteorology of the Southern Hemisphere*, *Meteor. Monogr.*, No. 49, Amer. Meteor. Soc., 89–99.

Moore, R. W., M. T. Montgomery, and H. Davies, 2013: Genesis criteria for diabatic Rossby vortices: A model study. *Mon. Wea. Rev.*, **141**, 252–263, doi:10.1175/MWR-D-12-00080.1.

Namias, J., 1939: The use of isentropic analysis in short term forecasting. *J. Aeronaut. Sci.*, **6**, 295–298, doi:10.2514/8.860.

Nieto, R., L. Gimeno, and R. M. Trigo, 2006: A Lagrangian identification of major sources of Sahel moisture. *Geophys. Res. Lett.*, **33**, L18707, doi:10.1029/2006GL027232.

O'Gorman, P. A., 2011: The effective static stability experienced by eddies in a moist atmosphere. *J. Atmos. Sci.*, **68**, 75–90, doi:10.1175/2010JAS3537.1.

Okumura, Y., and S.-P. Xie, 2004: Interaction of the Atlantic equatorial cold tongue and the African monsoon. *J. Climate*, **17**, 3589–3602, doi:10.1175/1520-0442(2004)017<3589:IOTAEC>2.0.CO;2.

Papritz, L., and T. Spengler, 2015: Analysis of the slope of isentropic surfaces and its tendencies over the North Atlantic. *Quart. J. Roy. Meteor. Soc.*, **141**, 3226–3238, doi:10.1002/qj.2605.

Parker, D. J., and Coauthors, 2005: The diurnal cycle of the West African monsoon circulation. *Quart. J. Roy. Meteor. Soc.*, **131**, 2839–2860, doi:10.1256/qj.04.52.

——, and A. J. Thorpe, 1995: Conditional convective heating in a baroclinic atmosphere: A model of convective frontogenesis. *J. Atmos. Sci.*, **52**, 1699–1711, doi:10.1175/1520-0469(1995)052<1699:CCHIAB>2.0.CO;2.

Pauluis, O., A. Czaja, and R. Korty, 2008: The global atmospheric circulation on moist isentropes. *Science*, **321**, 1075–1078, doi:10.1126/science.1159649.

Peixoto, J. P., and A. H. Oort, 1992: *Physics of Climate.* AIP Press, 520 pp.

Petterssen, S., and S. Smebye, 1971: On the development of extratropical storms. *Quart. J. Roy. Meteor. Soc.*, **97**, 457–482, doi:10.1002/qj.49709741407.

Pfahl, S., E. Madonna, M. Boettcher, H. Joos, and H. Wernli, 2014: Warm conveyor belts in the ERA-Interim dataset (1979–2010). Part II: Moisture origin and relevance for precipitation. *J. Climate*, **27**, 27–40, doi:10.1175/JCLI-D-13-00223.1.

——, P. O'Gorman, and M. Singh, 2015: Extratropical cyclones in idealized simulations of changed climates. *J. Climate*, **28**, 9373–9392, doi:10.1175/JCLI-D-14-00816.1.

Plant, R. S., G. C. Craig, and S. L. Gray, 2003: On a threefold classification of extratropical cyclogenesis. *Quart. J. Roy. Meteor. Soc.*, **129**, 2989–3012, doi:10.1256/qj.02.174.

Quaas, J., 2012: Evaluating the "critical relative humidity" as a measure of subgrid-scale variability of humidity in general circulation model cloud cover parameterizations using satellite data. *J. Geophys. Res.*, **117**, D09208, doi:10.1029/2012JD017495.

Ralph, F. M., P. J. Neiman, and G. A. Wick, 2004: Satellite and CALJET aircraft observations of atmospheric rivers over the eastern North Pacific Ocean during the winter of 1997/98. *Mon. Wea. Rev.*, **132**, 1721–1745, doi:10.1175/1520-0493(2004)132<1721:SACAOO>2.0.CO;2.

——, ——, G. N. Kiladis, and K. Weickmann, 2011: A multiscale observational case study of a Pacific atmospheric river exhibiting tropicalextratropical connections and a mesoscale frontal wave. *Mon. Wea. Rev.*, **139**, 1169–1189, doi:10.1175/2010MWR3596.1.

Rasmusson, E. M., 1967: Atmospheric water vapor transport and the water balance of North America: Part I. Characteristics of the water vapor flux field. *Mon. Wea. Rev.*, **95**, 403–426, doi:10.1175/1520-0493(1967)095<0403:AWVTAT>2.3.CO;2.

Rasmussen, E., 1979: The polar low as an extratropical CISK disturbance. *Quart. J. Roy. Meteor. Soc.*, **105**, 531–549, doi:10.1002/qj.49710544504.

Roebber, P. J., 1984: Statistical analysis and updated climatology of explosive cyclones. *Mon. Wea. Rev.*, **112**, 1577–1589, doi:10.1175/1520-0493(1984)112<1577:SAAUCO>2.0.CO;2.

Sadler, J. C., 1975: The upper tropospheric circulation over the global tropics. Tech. Rep. UHMET-75-05, Department of Meteorology, University of Hawaii, Honolulu, HI, 35 pp.

Salih, A. A. M., Q. Zhang, and M. Tjerström, 2015: Lagrangian tracing of Sahelian Sudan moisture sources. *J. Geophys. Res. Atmos.*, **120**, 6793–6808, doi:10.1002/2015JD023238.

Sanders, F., and J. R. Gyakum, 1980: Synoptic-dynamic climatology of the "bomb." *Mon. Wea. Rev.*, **108**, 1589–1606, doi:10.1175/1520-0493(1980)108<1589:SDCOT>2.0.CO;2.

Schultz, D. M., 2001: Reexamining the cold conveyor belt. *Mon. Wea. Rev.*, **129**, 2205–2225, doi:10.1175/1520-0493(2001)129<2205:RTCCB>2.0.CO;2.

Shapiro, M. A., and D. Keyser, 1990: Fronts, jet streams and the tropopause. *Extratropical Cyclones*, C. Newton and E. Holopainen, Eds., Amer. Meteor. Soc., 167–191.

Simmonds, I., R. J. Murray, and R. M. Leighton, 1999: A refinement of cyclone tracking methods with data from FROST. *Aust. Meteor. Mag.*, **48**, 35–49.

Sodemann, H., and A. Stohl, 2013: Moisture origin and meridional transport in atmospheric rivers and their association with multiple cyclones. *Mon. Wea. Rev.*, **141**, 2850–2868, doi:10.1175/MWR-D-12-00256.1.

Spengler, T., M. J. Reeder, and R. K. Smith, 2005: The dynamics of heat lows in simple background flows. *Quart. J. Roy. Meteor. Soc.*, **131**, 3147–3165, doi:10.1256/qj.04.177.

Stohl, A., C. Forster, and H. Sodemann, 2008: Remote sources of water vapor forming precipitation on the Norwegian west coast at 60°N—A tale of hurricanes and an atmospheric river. *J. Geophys. Res.*, **113**, D05102, doi:10.1029/2007JD009006.

Sultan, B., and S. Janicot, 2003: The West African monoon dynamics. Part II: The "preonset" and "onset" of the summer monsoon. *J. Climate*, **16**, 3407–3427, doi:10.1175/1520-0442(2003)016<3407:TWAMDP>2.0.CO;2.

Thorncroft, C. D., H. Nguyen, C. Zhang, and P. Peyrillé, 2011: Annual cycle of the west African monsoon: Regional circulations and associated water vapour transport. *Quart. J. Roy. Meteor. Soc.*, **137**, 129–147, doi:10.1002/qj.728.

Trenberth, K. E., J. T. Fasullo, and J. Mackaro, 2011: Atmospheric moisture transports from ocean to land and global energy flows in reanalyses. *J. Climate*, **24**, 4907–4924, doi:10.1175/2011JCLI4171.1.

Trier, S. B., C. A. Davis, D. A. Ahijevych, M. L. Weisman, and G. H. Bryan, 2006: Mechanisms supporting long-lived episodes of propagating nocturnal convection within a 7-day WRF model simulation. *J. Atmos. Sci.*, **63**, 2437–2461, doi:10.1175/JAS3768.1.

Troup, A. J., 1961: Variations in upper tropospheric flow associated with the onset of the Australian summer monsoon. *Indian J. Meteor. Geophys.*, **12**, 217–230.

Vera, C., and Coauthors, 2006: The South American low-level jet experiment. *Bull. Amer. Meteor. Soc.*, **87**, 63–77, doi:10.1175/BAMS-87-1-63.

Waliser, D. E., 1996: Formation and limiting mechanisms for very high sea surface tmperature: Linking the dynamics and thermodynamics. *J. Climate*, **9**, 161–188, doi:10.1175/1520-0442(1996)009<0161:FALMFV>2.0.CO;2.

Wernli, H., 1997: A Lagrangian-based analysis of extratropical cyclones. II: A detailed case-study. *Quart. J. Roy. Meteor. Soc.*, **123**, 1677–1706, doi:10.1002/qj.49712354211.

——, S. Dirren, M. A. Liniger, and M. Zillig, 2002: Dynamical aspects of the life cycle of the winter storm 'lothar.' *Quart. J. Roy. Meteor. Soc.*, **128**, 405–429, doi:10.1256/003590002321042036.

Wheeler, M., and J. L. McBride, 2005: Australian-Indonesian monsoon. *Intraseasonal Variability in the Atmosphere-Ocean Climate System*, W. K. M. Lau and D. E. Waliser, Eds., Praxis, 125–173.

Yamamoto, M., 2013: Effects of a semienclosed ocean on extratropical cyclogenesis: The dynamical processes around the Japan Sea on 23–25 January 2008. *J. Geophys. Res. Atmos.*, **118**, 10 391–10 404, doi:10.1002/jgrd.50802.

Yoshida, A., and Y. Asuma, 2004: Structures and environment of explosively developing extratropical cyclones in the northwestern Pacific region. *Mon. Wea. Rev.*, **132**, 1121–1142, doi:10.1175/1520-0493(2004)132<1121:SAEOED>2.0.CO;2.

Zhu, Y., and R. E. Newell, 1998: A proposed algorithm for moisture fluxes from atmospheric rivers. *Mon. Wea. Rev.*, **126**, 725–735, doi:10.1175/1520-0493(1998)126<0725:APAFMF>2.0.CO;2.